Objective Motion Cueing Criteria for Commercial Transport Simulators

Peter M. T. Zaal*
San Jose State University
NASA Ames Research Center
Moffett Field, CA, 94035

Jeffery A. Schroeder†
Federal Aviation Administration
Moffett Field, CA, 94035

William W. Chung‡
Science Applications International Corporation
NASA Ames Research Center
Moffett Field, CA, 94035

This paper adds data to establish fidelity criteria for the simulator motion system diagnostic test now required during commercial aircraft simulator approval in the United States. Nineteen airline transport pilots flew three tasks under six different motion conditions in an experiment on the NASA Vertical Motion Simulator. The motion conditions allowed refinement of the initial fidelity criteria developed in previous experiments. In line with these previous experiments, the motion condition significantly affected (1) false motion cue pilot ratings, and sink rate and longitudinal deviation at touchdown in the approach and landing task, (2) false motion cue pilot ratings, roll deviations, and maximum pitch rate in the stall task, and (3) false motion cue pilot ratings, heading deviation, and pedal reaction time after an engine failure in the take-off task. Combining data from three experiments, significant differences in pilot-vehicle performance were used to define objective motion cueing criteria boundaries. These fidelity boundaries suggest that some hexapod simulators can possibly produce motion cues with improved fidelity in several degrees of freedom.

Nomenclature

AFS	analogue fidelity scale rating, %	RMS_ϕ	RMS of roll deviation, deg
fx, fy, fz	surge, sway, heave specific force, ft/s^2	RMS_ψ	RMS of heading deviation, deg
g	gravitational acceleration, ft/s^2	s	Laplace variable
H	OMCT frequency response	t_p	pedal-response time, s
H_m	motion-filter frequency response	t_t	throttle-response time, s
H_{rt}	residual-tilt frequency response	V_2	takeoff safety speed, kts
H_{tc}	tilt-coordination frequency response	V_r	rotation speed, kts
$\dot{h}_{td}$	sink rate of main gear at touchdown, ft/s	V_{ref}	reference speed, kts
K_m	motion-filter gain	x, y, z	surge, sway, heave, ft
K_{rt}	residual-tilt gain	Δx_{td}	longitudinal touchdown deviation of main gear , ft
K_{tc}	turn-coordination gain		
N_1	engine fan speed, %	Δy_{td}	lateral touchdown deviation of main gear, ft
N_s	number of stick shakers		
p, q, r	roll, pitch, yaw rate, deg/s	ζ_m	motion-filter damping ratio
q_{max}	maximum pitch rate, deg/s	ω	frequency , rad/s
RMS_{gs}	RMS of glideslope deviation, dot	ω_m	motion-filter break frequency, rad/s
RMS_V	RMS of indicated airspeed deviation, kts	ω_{rt}	residual-tilt break frequency, rad/s

Abbreviations

CAVU	ceiling and visibility unlimited	LOC	localizer
FL	flight level	OMCT	Objective Motion Cueing Test
GS	glideslope	RMS	root mean square
ICAO	International Civil Aviation Organization	RWY	runway
		VMS	Vertical Motion Simulator

*Research Engineer, Mail Stop 262-2, peter.m.t.zaal@nasa.gov, Senior Member.
†Chief Scientific and Technical Advisor for Flight Simulation Systems, Mail Stop 243-5, jeffery.schroeder@faa.gov, Associate Fellow.
‡Simulation Engineer, Mail Stop 243-6, william.w.chung@nasa.gov, Senior Member.

I. Introduction

This paper adds data to results from three previous experiments[1–3] to develop motion fidelity criteria to accompany the diagnostic, specified in recent regulations and guidance, that quantifies simulator motion cues.[4,5] Actuator hardware and software algorithms determine motion cues. Since 2016, during simulator qualification, engineers measure the frequency response of the combined hardware and software system using an Objective Motion Cueing Test (OMCT).[4] However, the resulting measurements do not have accompanying metrics, or fidelity criteria, to assess their acceptability. That is because an international consensus has not been reached on what those metrics should be. Hosman et al. have documented OMCT results for a statistical sample of eight simulators to propose initial criteria,[6] which is useful, but having validated criteria would be an improvement.

Sinacori suggested simple criteria,[7,8] which are in reasonable agreement with much of the literature.[9–18] These criteria often necessitate motion displacements greater than most training simulators can provide. While some of the previous work has used transport aircraft in their studies, the majority used fighter aircraft or helicopters.[9–14] Those that used transport aircraft considered degraded flight characteristics.[15–18] So, it would be fair to say that earlier criteria lean more towards being sufficient, rather than necessary, criteria for typical transport aircraft training applications. Considering the prevalence of 60-inch, six-legged hexapod training simulators, a relevant question is "what are the necessary criteria that can be used with the OMCT?"

This research adds to the literature as follows. First, it examines well-behaved transport aircraft characteristics but in challenging flight tasks. Second, it adds six new motion configurations to the ten used in the highly similar tasks of the previous experiments, allowing for a comparison of pilot performance over a wide range of motion settings. Third, it uses the Vertical Motion Simulator (VMS), which allows for inclusion of relatively large motion conditions, much larger than typical training simulators can provide. Fourth, a sufficiently large pilot pool added statistical reliability to the results. Finally, the results of four experiments are combined to develop initial objective motion cueing criteria for commercial transport simulators.

The paper is structured as follows. The flight tasks and motion configurations are explained in Sections II and III, respectively. Section IV provides the experiment setup and hypotheses. Experiment results and OMCT criteria are presented and discussed in Sections V and VI, respectively, after which conclusions are drawn in Section VII.

II. Flight Tasks

The experiment had three tasks: an approach and landing with sidestep maneuver, a high-altitude stall recovery, and an engine-out after takeoff. The tasks were very similar to the tasks used in Refs. 1, 2, and 3. The assumption was that varying the motion cues would affect how pilots perform these challenging tasks. Fig. 1 shows the flight cards for the three tasks. Descriptions of each task and the aircraft model are provided in the following sections.

II.A. Approach and Landing with Sidestep

This task began at an altitude of 1,250 ft on a -3 deg glideslope approach to RWY 28R at San Francisco International Airport. Light turbulence, simulated using the Dryden turbulence model, existed throughout.[19] After breaking out of the cloud ceiling at 1,100 ft, air traffic control instructed the pilots to sidestep to RWY 28L. At a randomized height above ground level between 400 and 500 ft, a tail windshear of 15 kts was inserted by swiftly slewing the existing right quartering headwind (230/15) to a near tailwind (090/15). Pilots tried to maintain a -3 deg glideslope during the approach followed by landing within a 750-ft-long and 28-ft-wide box with a sink rate of 6 ft/s or less. An audio call-out began at a main gear height of fifty feet and repeated in decrements of 10 ft until touchdown. An overview of the runway configuration and definition of the touchdown box is given in Fig. 2.

This task evaluated if changes in motion cues affect 1) lateral-directional control in the sidestep maneuver, 2) speed and flightpath control along the glideslope and after the windshear, and 3) touchdown performance.

II.B. High Altitude Stall Recovery

The task started during cruise at 210 kts ($M = 0.75$) at an altitude of 41,000 ft. Pilots were instructed to initiate a self-induced stall by setting the throttles to idle, rolling 20 degs left or right and pitching approximately 15 degs nose up, decelerating through the stall warning until a negative sink rate was developed (as the aircraft model did not have a pronounced pitch break). The roll direction was determined randomly before the start of each run. To recover from the stall, pilots had to follow the correct recovery sequence of reducing the angle-of-attack (by pitching to approximately 15 deg nose down), leveling the wings, and applying full throttle until establishing a safe positive climb rate. The task

Task: approach to SFO RWY 28R with sidestep to landing on RWY 28L

Initial Condition: 1,250 ft altitude at V_{ref}+10=145 KIAS on GS and LOC for 28R

Configuration: gear down, flaps 30 deg, SB retracted

Ceiling/visibility: 1,100 ft ceiling, 10-mile visibility

Wind: 230/15 **Turbulence:** light

Gusts: windshear on final track

Procedure:

1. Track the GS and LOC to SFO RWY 28R maintaining 145 KIAS
2. Perform sidestep to RWY 28L at ATC command
3. Continue visual, tracking GS and LOC to RWY 28L
4. Recover from a tail windshear
5. Flare and touchdown 750 –1,500 ft from the threshold

Desired performance:

1. Deviation from 145 KIAS within $\pm$5 kts until 200 ft altitude
2. Glideslope deviation within $\pm$ one dot until 200 ft altitude
3. Longitudinal touchdown 750 –1,500 ft from threshold
4. Lateral touchdown $\pm$14 ft from centerline
5. Sink rate at touchdown $\leq$6 ft/s

(a) Approach and landing with sidestep

Task: recover from a high altitude stall

Initial Condition: level at FL 410 and 210 KIAS

Configuration: clean

Ceiling/visibility: CAVU

Wind: none **Turbulence:** moderate **Gusts:** none

Procedure:

1. Retard throttle to idle
2. Roll left or right (as indicated) to a 20 deg bank angle
3. Pull up to decelerate at approximately 4 kt/s
4. Continue deceleration through stick shaker until a sink rate develops
5. Apply nose down pitch, roll as needed, power as needed to return to steady-state flight

Desired performance:

1. Maintain bank angle within $\pm$5 degs about 20 degs during entry
2. Proper stall recovery procedure (push, roll, thrust, stabilized flight)
3. Recovers smoothly to speed $>$210 KIAS and positive rate of climb
4. Recover without exceeding airplane's limitations
5. Oscillatory load factor peaks between 0.75 and 1.25 g
6. Recover with smooth and positive control
7. During recovery, no more than one additional stick shaker activation

(b) High altitude stall recovery

Task: recover from engine out after takeoff

Initial Condition: at takeoff position on RWY 28R **Configuration:** gear down, flaps 10 deg

Ceiling/visibility: CAVU **Wind:** none **Turbulence:** none **Gusts:** none

Procedure:

1. Advance throttles to 60% N_1 with brakes engaged
2. Release brakes and advance throttles to 90% N_1
3. Maintain centerline
4. Rotate at V_r=128 kts, pitch to $\pm$ 12 degs and establish speed of V_2+15=150 KIAS
5. Confirm positive rate of climb and request gears up
6. Maintain heading and speed after single engine failure

Desired performance:

1. Desired heading $\pm$5 degs
2. Desired airspeed $\pm$5 kts
3. Bank approximately 5 degs towards operating engine

(c) Engine out after takeoff

Figure 1. Experiment flight cards.

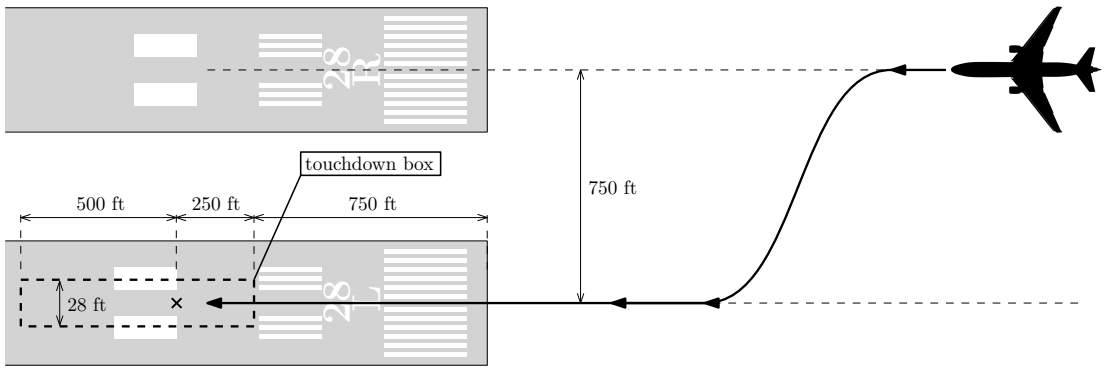

Figure 2. Runway configuration and touchdown box definition.

called for the pilots to pull the nose up gently and smoothly so as not to activate the stall warning during the recovery. Moderate turbulence was present.

This task evaluated if changes in motion cues affect the recovery performance by helping a pilot damp the flight path response, as well as stabilize the progressively less-stable roll dynamics near stall.

II.C. Engine Out after Takeoff

During the takeoff roll, the task required pilots to rotate at 128 kts, establish a 12 deg nose up pitch attitude, and maintain a steady climb speed of 150 kts. Either the left or right engine failed randomly at a random altitude after liftoff but below 100 ft. After identifying the failed engine, the pilots needed to apply near full rudder pedal towards the good engine, roll approximately 5 deg into the direction of the good engine to maintain the desired track, and modulate the remaining thrust to maintain speed.

This task evaluated if changes in motion cues affect a pilot's ability to detect the failed engine promptly and recover using appropriate lateral-directional control.

II.D. Aircraft Model

An existing mid-size twin-engine commercial transport aircraft model with a gross weight of 185,800 lbs was modified for this study. The enhancements allowed for a more representative aircraft response in the stall task. Most significantly, modifications to the lift coefficient as a function of angle of attack allowed for typical transport post-stall characteristics. Modifications to the rolling moment coefficient due to roll rate allowed for satisfactory representation of reduced roll stability near stall. Finally, modifications to the rolling moment coefficient due to aileron inputs allowed for an adequate representation of reduced roll control authority near the stall.

The simulated aircraft had six degrees of freedom and a two-crew cockpit. An unaugmented primary flight control system with actuator dynamics was used. The aircraft model included a landing gear model, allowing it to taxi, takeoff, and land. The aircraft could operate in the typical transport envelope up to a maximum cruising altitude of 42,000 ft.

III. Simulator Motion

Pilots performed each flight task with six motion configurations. The experiment used the standard VMS motion software algorithms and hardware for all motion configurations. The equivalent time delays of the VMS motion system for the pitch, roll, yaw, longitudinal, lateral, and vertical axes are 47, 68, 48, 50, 69, and 67 ms, respectively. More details about the VMS motion system and motion logic are provided in the appendix and in Ref. 20.

To compare the results of the current experiment against those of previous experiments in the remainder of this paper, the four motion configurations of the 2014 study, referred to as MCUE2014, are labeled M1-M4, and the six motion configurations of the 2015 study, referred to as MCUE2015, are labeled M5-M10. The six motion configurations of the current study (MCUE2016) are labeled M11-M16. The motion parameters for these six motion configurations are provided in the appendix. Motion configurations M11-M16 were kept as similar between tasks as possible; however, some variations between tasks were introduced to investigate specific task related motion effects. The main purpose of the current experiment was to reduce the initial OMCT fidelity boundary uncertainties found in the previous experiments.[3] Therefore, OMCT responses of M11-M16 were mostly inside these previously developed uncertainty boundaries.

Based on the results of the previous experiments, motion configurations were designed with three sub goals in mind. First, to further investigate the motion filter gain versus break-frequency trade-off, some configuration pairs differed in motion filter gain and others in break frequency only. Second, to investigate the relative importance of motion in degrees of freedom providing similar information to pilots (e.g., yaw and sway), some motion configuration pairs differed in motion fidelity in one degree of freedom, while motion fidelity in the related degree of freedom was kept constant at a lower fidelity level, and vice versa. Third, to refine the uncertainty boundaries of the cross-coupling OMCT responses, the magnitude of false tilt motion cues was varied systematically between motion configurations.

In the sidestep task, surge motion fidelity was thought to have an impact on pilots' ability to recover from the tail windshear. Roll motion fidelity, and, more specifically, the magnitude of the roll to sway response, was anticipated to influence pilots' perception of false tilt motion cues. Heave and pitch motion fidelity were believed to influence pilots' ability to address the sink rate during the flare. To investigate the effects stated above, the surge motion filter gain and break frequency were systematically increased going from M11 to M16; roll filter gain and break frequency were increased and decreased respectively, in an alternating fashion, to introduce decreasing levels of false tilt motion

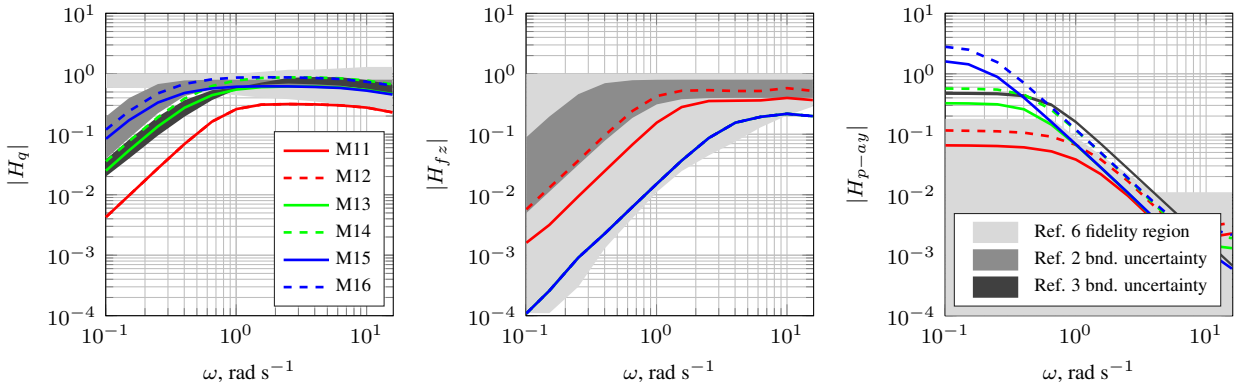

(a) Pitch response to pitch input. **(b) Heave response to heave input.** **(c) Sway response to roll input.**

Figure 3. Example of variations in OMCT responses for the stall task.

cues going from M11 to M16; and pitch and heave gains and break frequencies were varied with respect to each other resulting in increased pitch motion fidelity and decreased heave motion fidelity going from M11 to M16 (see Table 2).

In the stall task, roll motion fidelity was thought to influence pilots' ability to keep the desired roll angle and the perception of false tilt motion cues in the approach to the stall. Pitch and heave motion fidelity were thought to help pilots with regulating pitch oscillations in the stall recovery. The effects of roll motion were investigated by having the same variation in roll motion parameters as in the sidestep task. The relative effects of pitch and heave motion were investigated by varying heave gains and break frequencies in M11 and M12, while keeping pitch motion fidelity constant. M13-M16 had varying pitch gains and break frequencies while keeping heave motion fidelity constant.

Finally, in the takeoff task, the magnitude of the surge to pitch response (i.e., residual tilt) was thought to influence pilots' perception of false tilt motion cues in the initial takeoff run. Yaw and sway motion fidelity were anticipated to help pilots with addressing the yaw motion resulting from the engine failure. To investigate the effects of residual tilt, the residual-tilt break frequency was increased going from M11 to M16. The relative effects of yaw and sway motion were investigated by varying yaw gains and break frequencies in M11 and M12, while keeping sway motion fidelity constant. M13-M16 had varying sway gains and break frequencies while keeping yaw motion fidelity constant.

An example of the variations in OMCT responses between M11-M16 for the stall task is given in Fig. 3. Only the magnitudes of the responses are provided here. Furthermore, the low-pass characteristic of the pitch OMCT responses are omitted here for clarity. Fig. 3 also depicts the OMCT fidelity region developed in Ref. 6 and the fidelity uncertainty boundaries developed in the previous experiments for reference.[2,3] Figures 3a and 3b clearly show the alternating variation between pitch and heave motion fidelity. The gain and break-frequency trade off in pitch can also be observed. M13 and M15, and M14 and M16 had the same pitch motion gain; while M13 and M14, and M15 and M16 had the same filter break frequency. Fig. 3c shows the variation in magnitudes of the roll to sway motion responses introduced by the variation in roll motion filter parameters. At lower frequencies, M15 and M16 had roll to sway motion response magnitudes above the fidelity boundary found in the previous experiment, M13 and M14 had magnitudes around the previously found boundary, and M11 and M12 had magnitudes below the boundary.

IV. Experiment Setup

IV.A. Independent Variable

The only independent variable was the motion configuration, with six levels per task (M11-M16) (see Section III). Every pilot flew each of the three tasks with all six motion configurations.

IV.B. Apparatus

The experiment used the VMS with the transport cab (T-CAB) (Fig. 4).[20] Pilots flew from the left seat; the instructor occupied the right seat. A primary flight display (PFD) was positioned in front of each pilot (Fig. 5). The navigation displays were positioned next to the PFDs towards the center of the cab. An additional display in the center of the cab showed the engine parameters. This display changed to show task performance after each run.

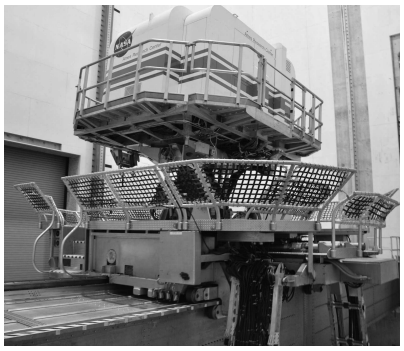

Figure 4. Vertical Motion Simulator.

Figure 5. Cockpit setup.

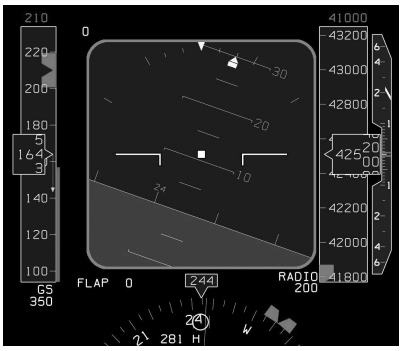

Figure 6. Primary flight display.

A column and wheel controlled aircraft pitch and roll, respectively. A thumb switch on the wheel controlled elevator trim. Conventional rudder pedals controlled the rudder deflection in the air and nose wheel steering on the ground. Two throttle levers controlled the thrust of the two engines. The instructor pilot configured flaps and gear with representative controls before each task.

The PFD symbology was similar to that on a Boeing 777 (Fig. 6). Speed and heading bugs indicated the desired speed and heading for each task. In addition, typical symbology on the speed tape indicated the minimum and maximum speeds, and V-speeds. The PFD also depicted conventional localizer and glide slope error indicators. A green speed trend vector originating from the indicated airspeed predicted what the airspeed would be in 10 s. The control columns in the cockpit had stick shakers to warn pilots of an impending stall. The activation of the shakers occurred simultaneously when the indicated airspeed coincided with the minimum speed tape, also known as the "barber pole".

The out-the-window visual cues of T-CAB were collimated and provided by a system that projected a high-quality image on six spherical mirrors. The mirrors formed a dome-like section providing a continuous field-of-view image to both pilots. The out-the-window visual had a 220° horizontal field of view and a 28° vertical field of view (10° up and 18° down). A Rockwell-Collins EPX5000 computer image generator created the out-the-window visual scene. The visual system equivalent time delay was 62 ms.[20] This was in line with the equivalent time delays of the motion system (Section III).

A Microsoft® Surface™ tablet was used by pilots to provide motion ratings.

IV.C. Procedures

The pilot pre-briefing explained the purpose of the experiment, the procedures, conditions, and performance criteria for each flight task. Pilots were informed they would perform each task with six different motion configurations and that the configurations would be presented randomly. However, no specifics about the motion configurations were given.

Pilots performed all three tasks, each with the six different motion configurations. Each motion configuration was repeated six times for a total of 36 runs per task. The first six runs were used as training runs in which the six motion conditions were presented once each. The remaining 30 runs were used for data analysis. A randomized Latin square determined the order of the tasks and motion configurations. All runs for a particular task were performed in a single session. Each session lasted one-and-a-half to two hours, and breaks were taken in between sessions.

Before each task, the instructor pilot reviewed the procedures, performance criteria, relevant controls, and displays. The instructor evaluated a pilot's performance after each run using task performance information displayed in the simulator cab. An experiment observer in the control room verified the evaluation. After completing each run, participant pilots rated the severity of false tilt motion cues during specific parts of the task with a rating scale on a tablet PC (Section IV.E).

IV.D. Participants

A total of 19 experienced airline transport pilots participated. All gave written consent for their participation. Fourteen pilots had a B757/B767 type rating, as the aircraft model used in the simulation was of an aircraft similar to a B757 in terms of configuration, size, and weight. Most pilots had experience on many other commercial transport aircraft types. The average number of flying hours pilots had on a B757/B767 was 4,282 with a standard deviation of $\pm$3,943. The average number of flying hours on other aircraft types was 7,839 with a standard deviation of $\pm$5,855.

All pilots were male and twelve had experience as a captain. Twelve pilots had also participated in the previous experiments.[2,3]

IV.E. Dependent Measures

Three subjective dependent measures and 12 objective dependent measures were recorded and analyzed. Pilots rated the severity of false tilt motion cues in each task by moving a digital slider on an analogue fidelity scale (AFS) after each run. The analogue scale ranged from 0% (not noticeable) to 100% (very obvious and objectionable). In the sidestep and stall tasks, pilots were asked to rate the severity of false tilt cues during the turns often experienced by leaning to one side or moving laterally in the seat. In the takeoff task, pilots rated the severity of false tilt cues at the start of the takeoff run often experienced by a mismatch between visual and motion cues, resulting in an uneasy feeling.

Several objective measures determined the effect of motion on task performance. Many measures related directly to the performance criteria (Fig. 1). For the approach and landing with sidestep, the RMS of the glide slope, RMS_{gs}, and speed deviation, RMS_V, after the wind shear were calculated. Calculations for these variables used data from the first 10 s after the wind shear was initiated. The reaction time of the throttle input after the wind shear, t_t, was from the time of the start of the wind shear to the time when the throttle input reached its maximum. When the main gear touched the runway, data captures occurred for the sink rate, $\dot{h}_{td}$, and the longitudinal and lateral deviations, Δx_{td} and Δy_{td}, from the desired touchdown point.

For the stall recovery, the RMS roll error, RMS_ϕ, applied to the 30 s before the start of the stall recovery. The maximum pitch rate deviation, q_{max}, and the number of stick shakers, N_s, applied to the stall recovery segment. Pitch rate was substituted as a partial surrogate to analyze load factor oscillations in the stall recovery, as it was more suitable for analyzing oscillatory behavior. Finally, for the engine out after takeoff task, the RMS of the heading and speed deviations after the engine failure, RMS_ψ and RMS_V, used data from the first 15 s after the engine failure. The reaction time of the initial pedal input after the engine failure, t_p, was from the time of the engine failure to the time when the pedal input was 10% of the maximum input.

Table 1. Summary of statistical test results.

Measure	*df*	F/χ^2	p	η^2	Sig.
Sidestep Task					
AFS	$1.8, 8.9^{gg}$	5.680	0.028	0.532	$**$
RMS_{gs}	5.0, 90.0	0.811	0.545	0.043	–
RMS_V	5.0, 90.0	0.260	0.933	0.014	–
t_t	$3.8, 68.9^{gg}$	1.608	0.184	0.082	–
$\dot{h}_{td}$	5.0, 90.0	17.408	0.000	0.492	$**$
Δx_{td}	$3.4, 61.1^{gg}$	2.250	0.084	0.111	$*$
Δy_{td}	$2.6, 46.7^{gg}$	1.684	0.189	0.086	–
Stall Task					
AFS	$1.5, 7.3^{gg}$	5.752	0.038	0.535	$**$
RMS_ϕ	5.0, 90.0	7.549	0.000	0.295	$**$
q_{max}	$2.5, 44.4^{gg}$	5.531	0.004	0.235	$**$
N_s	5.0	9.054	0.107	–	–
Takeoff Task					
AFS	$1.9, 9.7^{gg}$	4.556	0.041	0.477	$**$
RMS_ψ	5.0, 90.0	3.641	0.005	0.168	$**$
RMS_V	$2.9, 52.4^{gg}$	1.269	0.294	0.066	–
t_p	$3.2, 57.5^{gg}$	10.619	0.000	0.371	$**$

gg = Greenhouse-Geisser correction
$**$ = significant ($p < 0.05$)
$*$ = marginally significant ($0.05 \leq p < 0.1$)
– = not significant ($p \geq 0.1$)

V. Results

Mean task performance results from the current experiment are from 19 pilots for the approach and landing with sidestep, high-altitude stall recovery, and engine out after takeoff tasks. For the motion ratings, data from six pilots was collected only due to an error in the motion rating software. For every pilot, data from the last five runs for each task and motion configuration were averaged. Error-bar plots present the continuous-interval dependent measures, with means and 95% confidence intervals for each motion condition. Bar plots present the ordinal dependent measures, with the number of occurrences for each dependent measure level and the median for each motion condition. Wherever appropriate, gray dashed lines depict the task performance criteria. Task performance results of the previous two experiments (MCUE2014 and MCUE2015) are provided on the left side of each figure for reference, but are not discussed in detail. Task-performance results for the current experiment (MCUE2016) are depicted on the right side.

A repeated-measures analysis of variance (ANOVA) detected statistically significant differences in the continuous interval dependent measures (Table 1).[21] A Friedman test was used for the ordinal dependent measures. For the ANOVA to produce accurate results, the data must meet three assumptions: 1) there should be no significant outliers, 2) data should be approximately normally distributed for each level of the independent variable, and 3) variances

of the differences between all combinations of levels of the independent variable must be equal (i.e., assumption of sphericity).

Box plots identified outliers, normality was checked using the Shapiro-Wilk test, and Mauchly's test checked the assumption of sphericity. Few outliers were detected, so they were kept in the data analysis. Data were generally normally distributed. In the few cases they were not, we did not correct for it, as an ANOVA is fairly robust to deviations from normality. When the assumption of sphericity was violated, the degrees of freedom of the ANOVA were corrected using the Greenhouse-Geisser adjustment.

Post-hoc tests with Bonferroni adjustment were performed for pairwise comparisons of motion conditions when the ANOVA indicated an overall significant difference. All statistical tests had a significance level of 0.05. Table 1 gives a summary of the statistical test results for all the repeated measures (Section IV.E). In this table, df are the degrees of freedom, F or χ^2 is the test statistic for the ANOVA or Friedman test, respectively, p is the probability of observing an effect, and η^2 is the partial eta-squared, indicating sample effect size.

Task-performance results for each task are provided first, followed by an analysis of the magnitude of false tilt motion cues and the motion ratings. Finally, objective motion cueing criteria developed using the task-performance and motion-rating results from the last three experiments are presented.

V.A. Task Performance Results

V.A.1. Approach and Landing with Sidestep Task

Figures 7 to 9 provide the task performance results for the approach and landing with sidestep task. The RMS of the glideslope and speed deviation in the approach are given in Fig. 7. No significant differences were found between conditions for both variables (Table 1). Note that pilots were able to meet the glideslope-deviation performance requirement easily in previous experiments with an average glideslope deviation of around 0.4 dots. Glideslope deviations were slightly higher in the current experiment as a result of the additional windshear. Pilots had difficulties meeting the speed-deviation performance requirement with average airspeed deviations between 5 and 6 kts in previous experiments, and deviations around 14 kts in the current experiment. The large increase in overall speed deviation in MCUE2016 was introduced by the windshear as well.

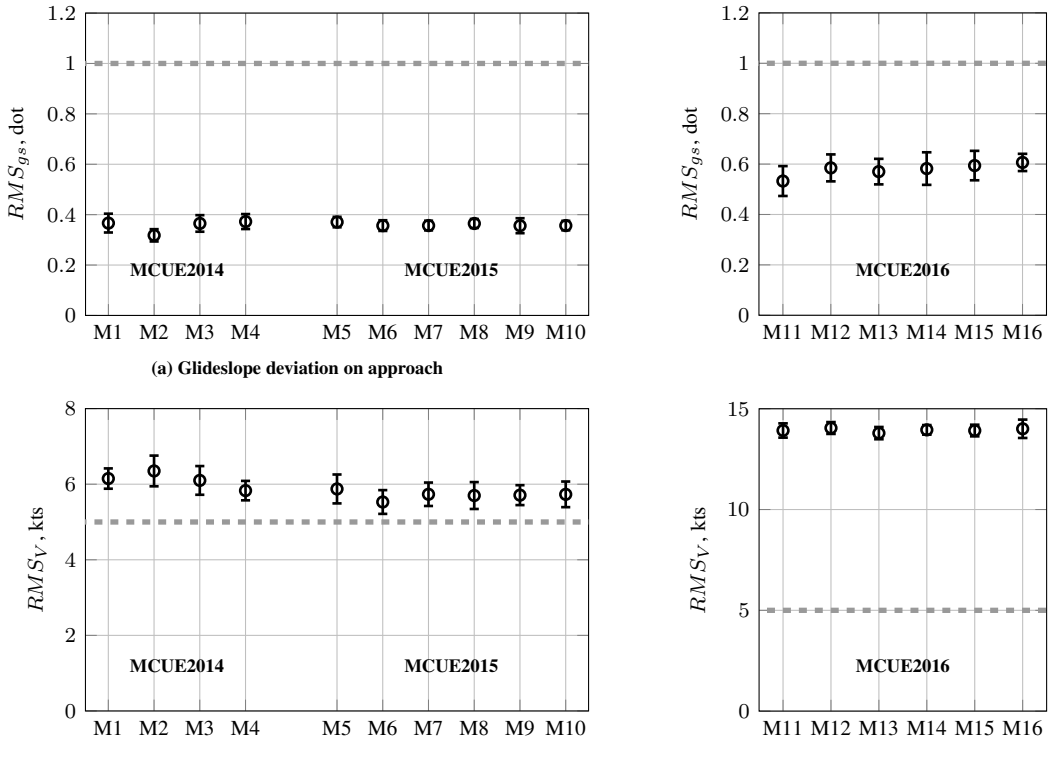

(a) Glideslope deviation on approach

(b) Speed deviation on approach

Figure 7. Approach performance data of the approach and landing with sidestep task.

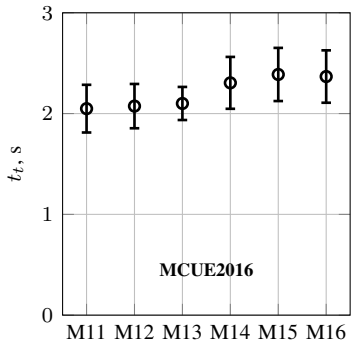

Figure 8. Throttle reaction time after the windshear onset.

Fig. 8 depicts the throttle reaction time t_t after the onset of the windshear. The throttle reaction time was not significantly different between motion configurations. It took pilots around 2.0-2.5 s to apply full throttles after the onset of the windshear to correct for the significant drop in airspeed.

Touchdown performance is provided in Fig. 9. The sink rate at touch down, depicted in Fig. 9a, was statistically significantly different between motion configurations (Table 1). Post-hoc analysis with Bonferroni adjustment revealed that the sink rate at touchdown in motion configuration M16 was significantly higher than M11 ($p < 0.001$) and M12 ($p = 0.008$), in M15 was significantly higher than M11 ($p < 0.001$) and M12 ($p = 0.001$), in M14 was significantly higher than M11 ($p < 0.001$) and M12 ($p < 0.001$), and M13 was significantly higher than M11 ($p = 0.003$). Finally, the sink rate was marginally significantly higher in M15 compared to M13 ($p = 0.062$). The average sink rate at touchdown was around the maximum allowable value of 6 ft/s for M14-M16 and very similar to the average sink rate in the hexapod motion configurations of MCUE2014 (M2-M4) and the motion configurations of MCUE2015 (M5-M10). The sink rate at touchdown in M11 was very similar to the sink rate in the large-motion configuration M1.

Fig. 9b depicts the longitudinal deviation from the desired touchdown point. This performance metric was marginally significantly different between motion configurations. The longitudinal deviation from the desired touchdown point increased from M11 to M16. Post-hoc analysis with Bonferroni adjustment revealed that the longitudinal deviation in motion configuration M16 was marginally significantly higher than M11 ($p = 0.063$). Pilots generally touched down around the maximum allowable 1,500 ft from the runway threshold in the current experiment, similarly to MCUE2014. Pilots touched down well before the limit in MCUE2015, around 1,250 ft.

The lateral deviation from the desired touchdown point was not significantly different between motion configurations (Fig. 9c). Pilots touched down around 4 ft from the centerline laterally on average. In previous experiments, pilots deviated much more from the centerline due to turbulence implementation issues.[3]

V.A.2. High-Altitude Stall Recovery Task

The task-performance results for the high-altitude stall recovery task are depicted in Fig. 10. The RMS roll deviation in the approach to the stall was significantly different between motion conditions (Fig. 10a). Post-hoc analysis with Bonferroni adjustment revealed that the RMS roll deviation in M11 was significantly higher than in M14 ($p = 0.016$), M15 ($p = 0.042$), and M16 ($p = 0.022$). The roll deviation in M12 was singificantly higher than in M14 ($p < 0.001$) and M15 ($p = 0.007$), and marginally significantly higher than in M16 ($p = 0.063$). Note that pilots stayed well below the maximum allowable roll deviation in all conditions. RMS roll deviations were similar in all three experiments.

Fig. 10b depicts the maximum pitch rate deviation during the stall recovery, which increased from M11 to M16. The main ANOVA found that this variable was statistically significantly different between conditions. Post-doc analysis with Bonferroni adjustment found that this significant test result was due to a marginal significant difference between M12 and M16 ($p = 0.053$).

The bars in Fig. 10c indicate the number of times a pilot activated 0, 1, 2, 3, or 4 additional stick shakers during the stall recovery. Medians of the data are depicted by the dashed horizontal lines. A Friedman test did not reveal any significant differences between conditions. Note that more additional stick shakers were triggered in the MCUE2015 and MCUE2016 experiments compared to MCUE2014. At most, two stick shakers were triggered in each condition of MCUE2014, while in some conditions of MCUE2015 and MCUE2016 up to four stick shakers were triggered.

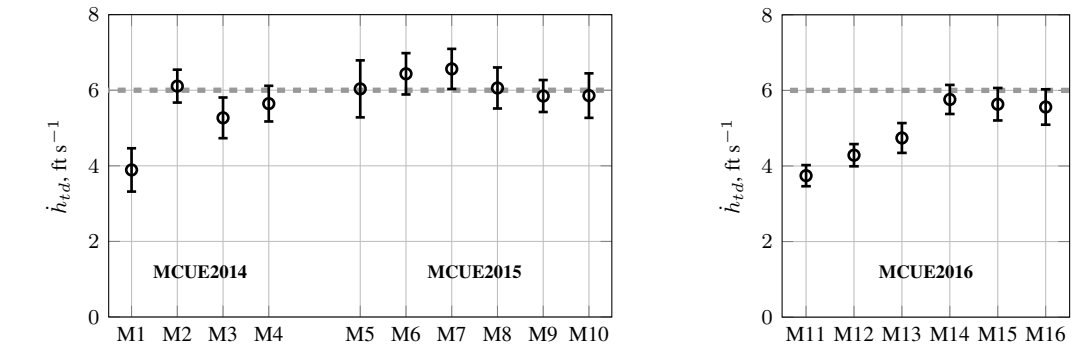

(a) Vertical speed at touchdown

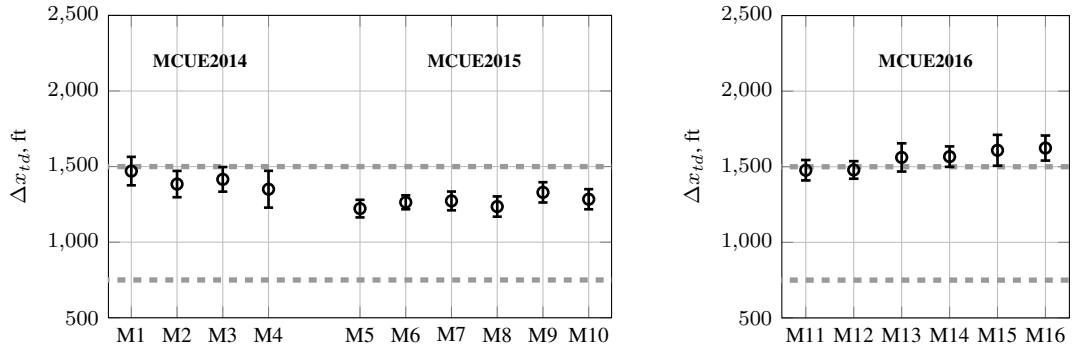

(b) Longitudinal deviation from touchdown point

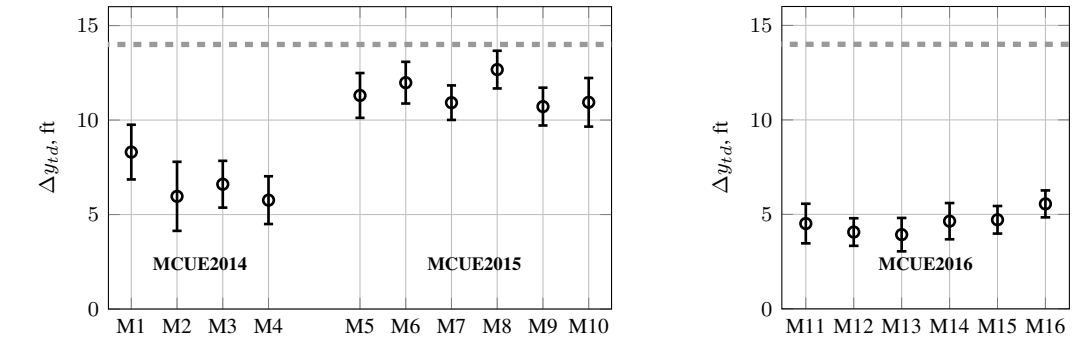

(c) Lateral deviation from touchdown point

Figure 9. Touchdown performance data of the approach and landing with sidestep task.

V.A.3. Engine Out after Takeoff Task

Task performance for the engine out after takeoff task is depicted in Fig. 11. The RMS heading deviation after the engine failure was statistically significantly different between motion configurations and increased from M11-M12 to M13, and then decreased towards M16 (Fig. 11a). Post-hoc analysis with Bonferroni adjustment revealed that RMS heading deviation in condition M13 was significantly higher than M11 ($p = 0.006$), M12 ($p = 0.004$), and M16 ($p = 0.034$). When compared to the previous experiments, RMS heading deviation in MCUE2016 was very similar to that in M2-M4 and M7-M10 of the previous experiments. Pilots were able to easily meet the heading performance criterion.

The RMS speed deviation after the engine failure is depicted in Fig. 11b. The ANOVA did not detect any significant differences between motion configurations. The average RMS speed deviation was similar to MCUE2015 and lower compared to MCUE2014. Note that pilots were able to meet the speed performance criterion with ease.

Fig. 11c depicts the reaction time of the initial pedal input after the engine failure. The ANOVA detected significant differences between motion configurations. Post-hoc analysis revealed that the reaction time in M16 was statistically significantly lower than in M13 ($p < 0.001$), M14 ($p = 0.012$), and M15 ($p = 0.002$), and marginally significantly

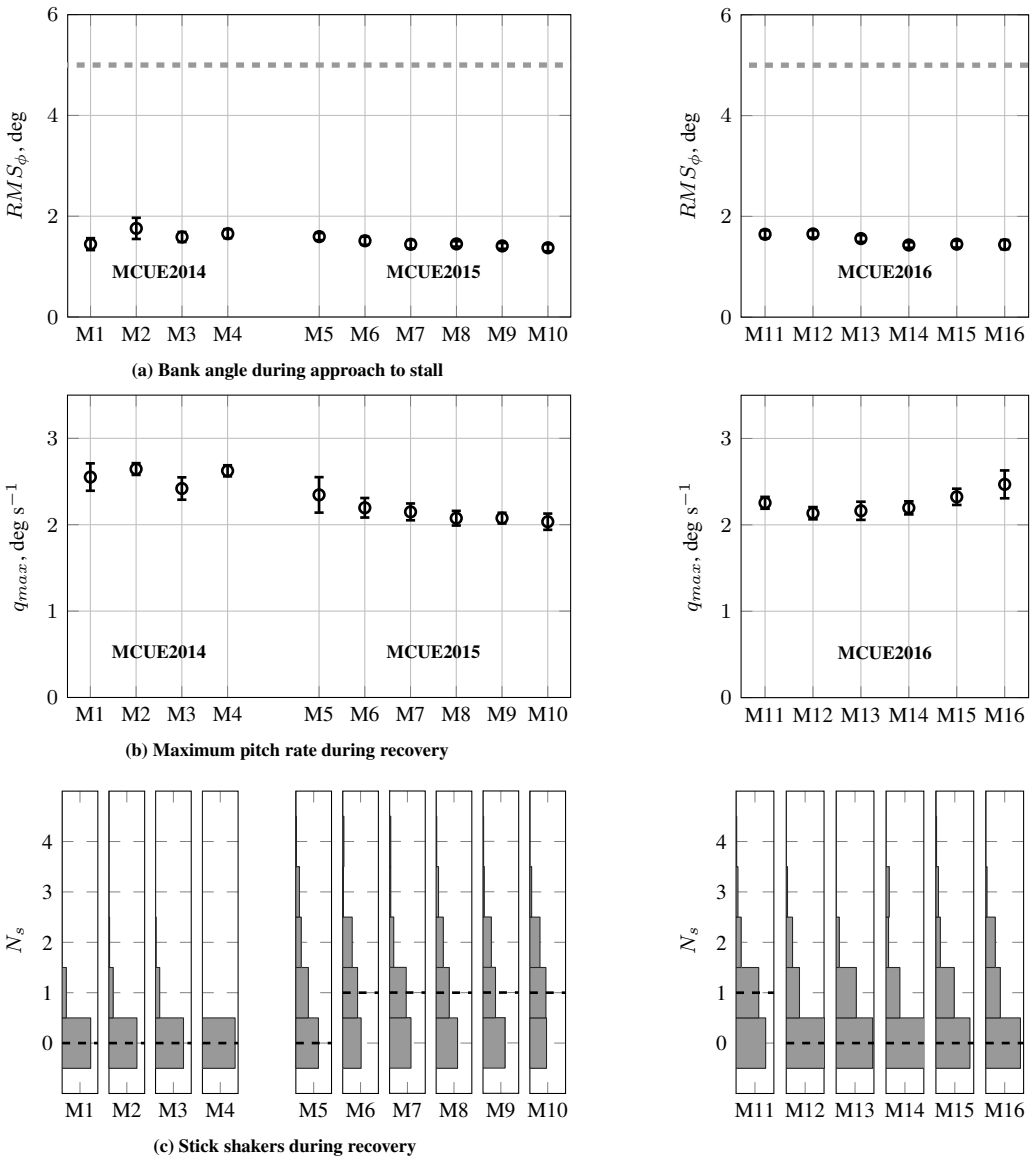

(a) Bank angle during approach to stall

(b) Maximum pitch rate during recovery

(c) Stick shakers during recovery

Figure 10. Performance data of the high altitude stall recovery task.

lower than in M11 ($p = 0.059$) and M12 ($p = 0.070$). The reaction time in M12 was marginally significantly lower than in M13 ($p = 0.078$). Note that the pedal reaction time follows a similar pattern compared to the RMS heading deviation; that is, increased from M11-M12 to M13-M15 and then decreased to M16. Values were between 1.5 and 2.0 s in all three experiments.

V.B. False-Tilt-Motion Cues

V.B.1. Magnitude

The magnitude of false tilt motion cues was determined in the sidestep, stall, and takeoff tasks. More specifically, the maximum lateral specific force due to insufficient turn coordination was determined in the sidestep maneuver from runway 28R to 28L and the turn in the approach to stall, while the maximum pitch rate due to residual tilt was determined in the initial takeoff run.

In a coordinated turn, there is no lateral specific force. In a simulator, even when the model also does not have a lateral specific force in a coordinated turn, if the simulator cab rolls (say to the right), the simulator must accelerate to the right (in the sway degree of freedom) so that the simulator pilot does not feel a false lateral specific force. Limited

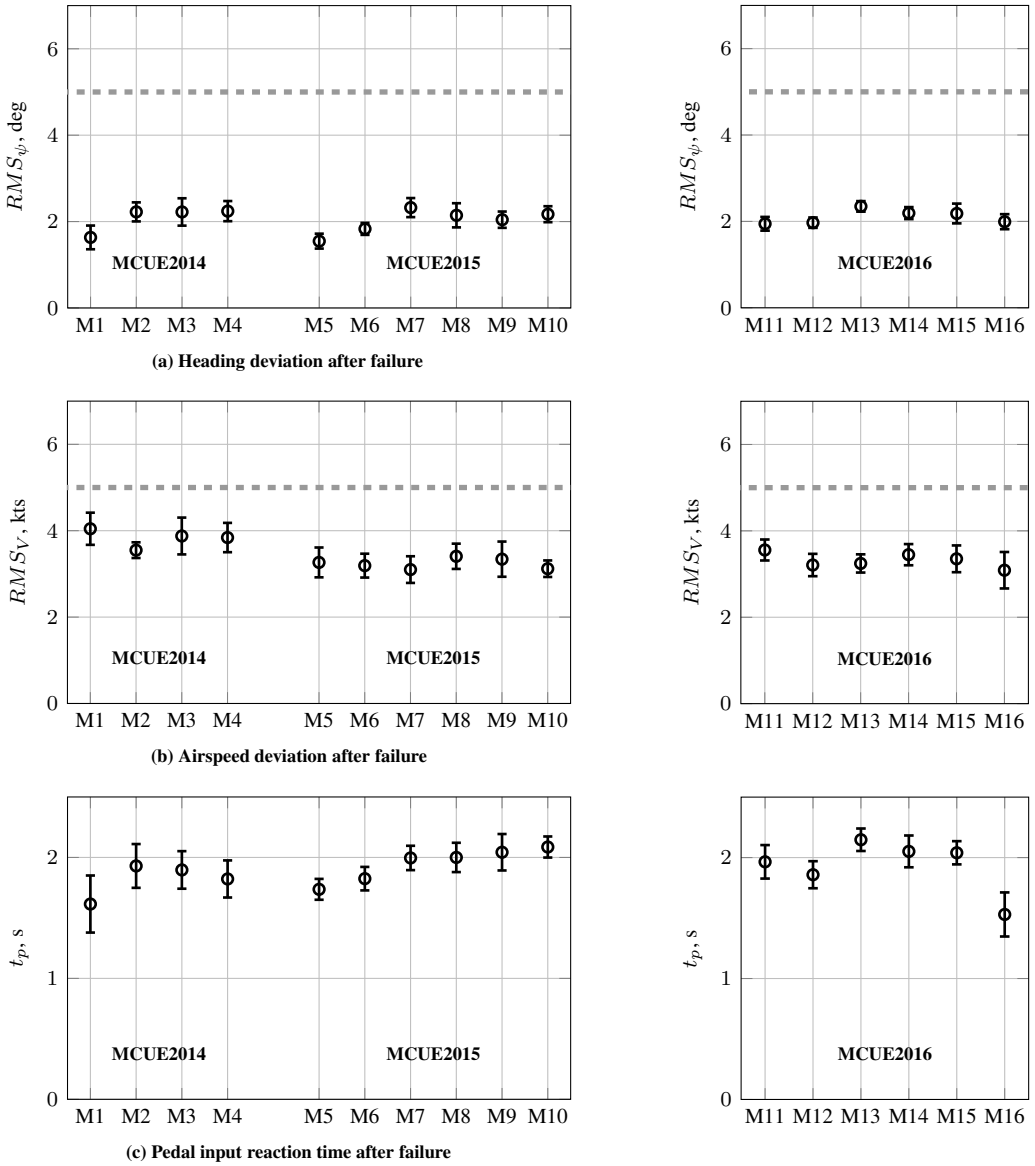

(a) Heading deviation after failure

(b) Airspeed deviation after failure

(c) Pedal input reaction time after failure

Figure 11. Performance data of the engine out after takeoff task.

sway motion in a simulator prevents the elimination of this false cue, and it results in the pilot feeling the leans. Jex et al. found that peak lateral specific forces with a magnitude above 0.1 g resulted in consistent pilot comments about false tilt cues.[14] Fig. 12a depicts the maximum lateral specific force due to roll in the aircraft body reference frame before reaching the decision altitude of 200 ft in the sidestep task for all three experiments (MCUE2014, MCUE2015, and MCUE2016). The dashed gray line indicates a specific force of 0.1 g. Note that the lateral specific forces in Fig. 12a are a result of the motion logic settings in the different motion configurations and also pilots' performance; that is, if roll angles remain smaller due to smaller wheel inputs, lateral specific forces remain smaller as well.

Fig. 12a shows that the maximum lateral specific forces due to roll stayed well below the 0.1 g level for MCUE2015. For MCUE2014 and MCUE2016, the turn-coordination channel of the VMS motion logic was purposely turned off, resulting in much higher maximum lateral specific forces. The highest maximum lateral specific force due to roll was obtained for the full-motion condition M1 in MCUE2014. The maximum lateral specific force in condition M4 was just at the 0.1 g level. For MCUE2016, motion logic parameters were chosen such that there was a gradual increase in the magnitude of false tilt cues going from M11 to M16. For M11 to M15, the maximum lateral specific force remained below the 0.1 g perception threshold, while for M16 it was above the threshold.

Fig. 12b depicts the maximum lateral specific force due to roll before stall in the stall task. Again, the dashed gray line indicates a specific force of 0.1 g, the perception threshold of false-tilt motion cues found in previous research.

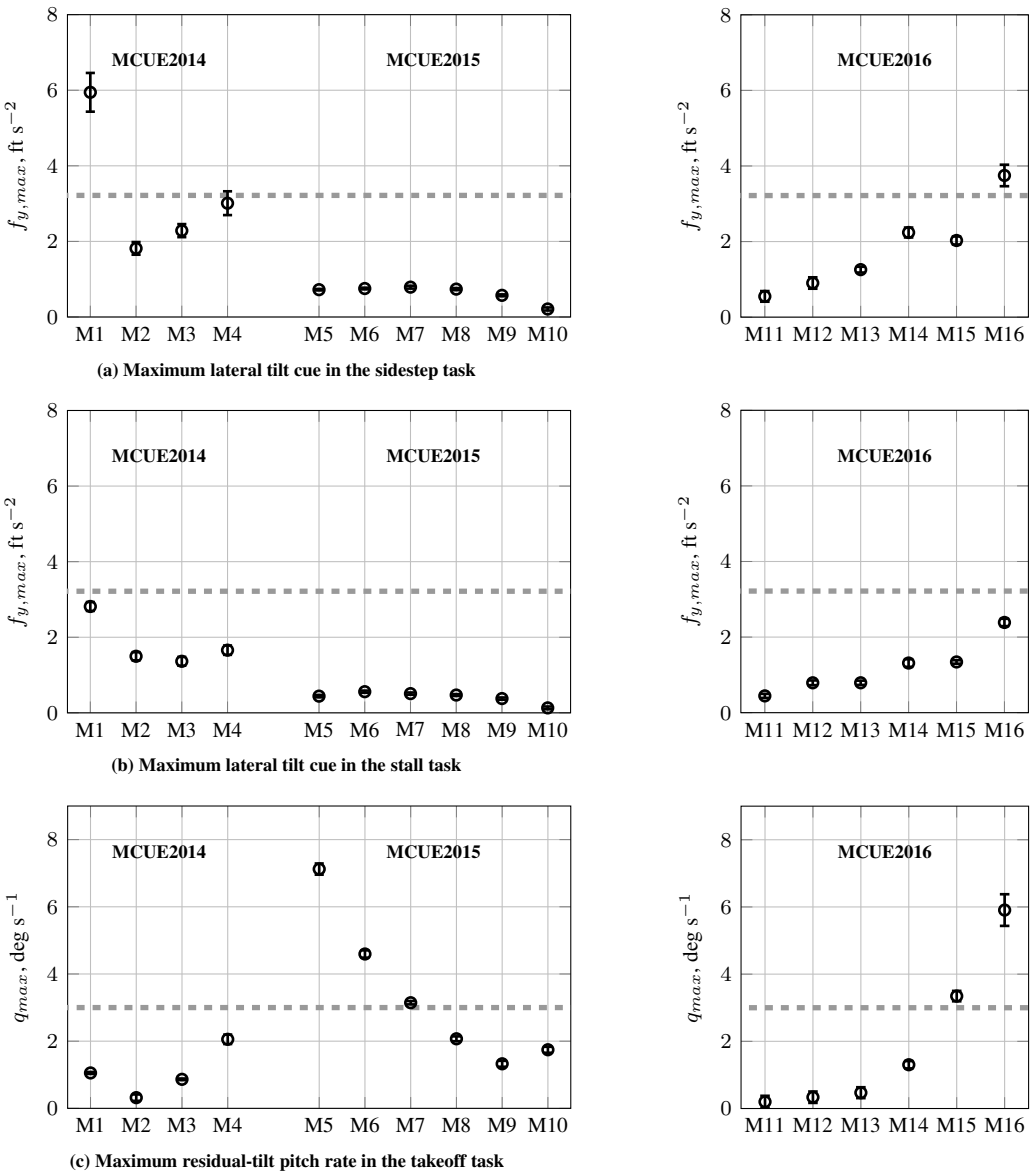

(a) Maximum lateral tilt cue in the sidestep task

(b) Maximum lateral tilt cue in the stall task

(c) Maximum residual-tilt pitch rate in the takeoff task

Figure 12. False motion cues.

For all experiments, the maximum lateral specific force due to roll stayed below the 0.1 g threshold. The maximum lateral specific force is higher for MCUE2014 and MCUE2016 as the turn-coordination channel of the VMS motion logic was not used in these experiments. Motion configuration M1 in MCUE2014 and M16 in MCUE2016 produced maximum lateral specific forces close to the 0.1 g perception threshold.

Residual tilt is the process of tilting the simulator cab to provide steady-state longitudinal and lateral accelerations at low frequencies. Groen et al. determined that whole-body tilt improves motion fidelity of visually simulated linear motion; however, rotational rates should not exceed approximately 3 deg/s.[22] Fig. 12c depicts the maximum pitch rate due to residual tilt at the start of the takeoff roll. The dashed gray line indicates a rotational rate of 3 deg/s. Note that the rotational rates in Fig. 12c are also a combination of the motion logic settings in the different motion configurations and pilot inputs. The pitch rates remain smaller if the throttles are advanced more slowly. The maximum pitch rate due to residual tilt stayed well below the 3 deg/s level for all conditions in MCUE2014. For MCUE2015, the maximum pitch rate due to residual tilt decreased from M5 to M10. The highest maximum value was obtained for condition M5. The maximum pitch rate increased going from M11 to M16 in MCUE2016. The maximum pitch rate in conditions M7 and M15 was approximately at the 3 deg/s perception threshold.

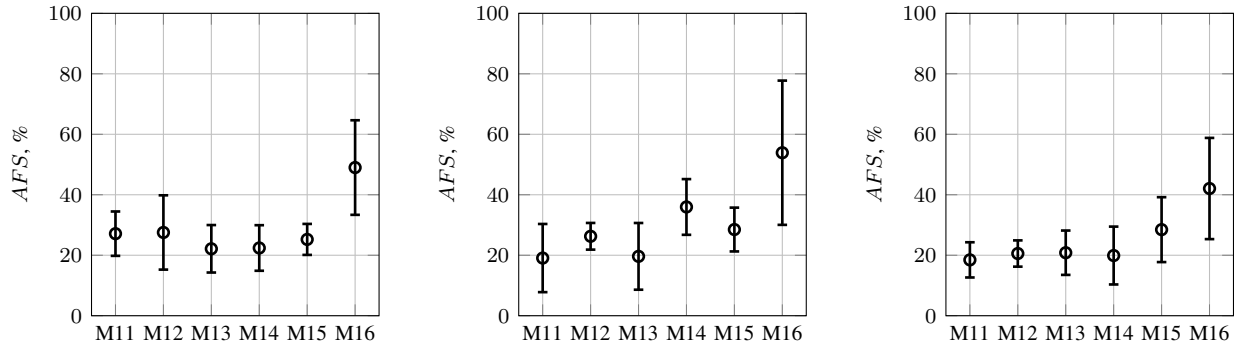

(a) Approach and landing with sidestep maneuver **(b) High-altitude stall recovery** **(c) Engine out after takeoff**

Figure 13. MCUE2016 motion rating data.

V.B.2. Ratings

In MCUE2016, pilots rated the severity of false tilt motion cues during each task by moving a slider on an analogue fidelity scale between 0% and 100% (Section IV.E). The resulting ratings AFS are depicted in Figures 13a, 13b, and 13c for the sidestep, stall, and takeoff tasks, respectively.

The repeated-measures ANOVA revealed that the false-tilt-motion-cue ratings were significantly different between motion configurations in the sidestep task (Table 1). A post-hoc analysis with Bonferroni adjustment revealed the severity of false tilt motion cues in the sidestep maneuver was rated significantly higher, at 50%, in M16 compared to 28% in M11 ($p = 0.050$). No significant differences were found between any of the other motion configurations. Motion ratings in M11-M15 were similar and around 25%. Note that the maximum lateral specific force due to roll in M16 was above the human perception threshold found in previous studies and remained below it for all other motion configurations (Fig. 12a), indicating that the ratings found here are in agreement with those studies.

The false-tilt-motion-cue ratings were also significantly different between motion configurations in the stall task. However, Post-hoc analysis with Bonferroni adjustment revealed no significant differences between any motion condition pairs. Due to the conservative nature of the Bonferroni adjustment, pairwise comparisons were also performed without any correction. This revealed significantly higher ratings in M16 compared to M11 ($p = 0.044$), M12 ($p = 0.052$), and M13 ($p = 0.046$), and significantly higher ratings in M14 compared to M12 ($p = 0.052$). The maximum lateral specific force due to roll in M16 was around the human perception threshold determined previously and remained below it for all other conditions (Fig. 12b), again indicating that the ratings found here show good correlation with previous research.

Finally, the false-tilt-motion-cue ratings were significantly different between motion configurations in the takeoff task. Post-hoc analysis with Bonferroni adjustment revealed no significant differences between any motion condition pairs. Pairwise comparisons without any correction revealed significantly higher ratings in M16 compared to M11 ($p = 0.034$), M12 ($p = 0.046$), and M13 ($p = 0.040$). Note that the maximum pitch rate due to residual tilt in M16 was well above the human perception threshold found in previous studies, was around the threshold in M15, and remained below it for M11-M14 (Fig. 12a), indicating that the ratings found here are in reasonable agreement with those studies.

V.C. Motion Cueing Criteria

Statistical differences in task performance and false-motion-cue ratings between the motion configurations were used to refine the initial objective motion cueing criteria boundaries developed in the previous studies (MCUE2014 and MCUE2015). The same general procedure was followed as in Refs. 2 and 3. ANOVAs revealed nine dependent variables were statistically significantly different between motion configurations: the false tilt motion cue ratings AFS for all three tasks, the vertical speed at touchdown $\dot{h}_{td}$ and the longitudinal deviation from the desired touchdown point Δx_{td} in the sidestep task, the RMS roll deviation RMS_ϕ and the maximum pitch rate q_{max} in the stall task, and the RMS heading deviation RMS_ψ and the pedal reaction time t_p in the takeoff task (see Table 1). These results are in line with the previous experiments.

Using data from all three experiments, motion fidelity boundaries were defined by assigning a task performance result to each principal degree of freedom. Task performance results were used to define the boundaries for the high-

pass filter portion of the principal motion responses only. False motion cue ratings were used to define boundaries for the cross-coupling between degrees of freedom. These boundaries were also used as the boundaries for the low-pass characteristic in the pitch, surge, and sway principal degrees of freedom. Using significant differences in task performance or motion ratings between different motion configurations, fidelity boundaries were defined using the OMCT responses of those motion configurations. If motion configurations mainly differed in motion filter gain, that is, the motion filter break frequency between the two conditions was similar, the OMCT responses were used to suggest fidelity boundaries for magnitude only. Similarly, if motion configurations mainly differed in motion filter break frequency, the OMCT responses were used to suggest fidelity boundaries for phase only. Motion configurations that differed significantly in both gain and break frequency were used in both magnitude and phase plots when significant differences arose in the objective or subjective measures. Gains were deemed similar when they differed less than 0.15 and break frequencies were deemed similar when they differed less than 0.15 rad/s.

An example of applying the above strategy is provided in Fig. 14 which shows how the heave fidelity magnitude boundaries were developed using the following steps:

1. Sink rate at touchdown in the sidestep task was used to develop heave OMCT fidelity boundaries. As indicated in Fig. 14a, sink rate at touchdown was significantly different between M1, and M2, M3, and M4 in MCUE2014. The motion filter gains between M1 and M4 were similar.[2] Therefore, for the magnitude plot, we assumed that a fidelity boundary exists between the OMCT responses of the remaining motion-configuration pairs only (M1 and M2, and M1 and M3).

2. Fig. 14b shows the magnitude of the objective motion cueing test responses for M1-M3. The areas between the responses, containing a possible fidelity boundary, are marked in light gray. In the region where both areas overlap, resulting in a darker gray, the final fidelity boundary exists. This overlapping area is the fidelity boundary uncertainty area. Adding results from additional experiments further refined the fidelity boundary uncertainty area; that is, reduced the width of the dark-gray area.

3. Among other condition pairs not depicted here for clarity, significant differences in sink rate at touchdown were also found between M12 and M14 in MCUE2016, further reducing the width of the uncertainty area (Fig. 14c). After combining the results from three experiments, the edges of the remaining uncertainty boundary area were fit by an analytically calculated heave motion response taking into account both magnitude and phase. These fits, shown in red in Fig. 14c, ensured that the uncertainty boundary area is confined by responses that are physically possible based on the structure of the motion logic used. The area confined by the response fits is the final uncertainty boundary area containing the motion fidelity boundary.

4. Finally, being on the conservative side, the lower edge of the boundary uncertainty area, indicated by the red continuous line, was chosen as the final motion fidelity boundary. This motion fidelity boundary defines one side of a satisfactory motion fidelity region. The other side of the region is defined by the magnitude-of-one or zero-phase-error lines.

The four steps above describe the main approach used to define the motion fidelity boundaries for the principal high-pass filter responses using significant differences in task performance. Boundaries for the cross-coupling re-

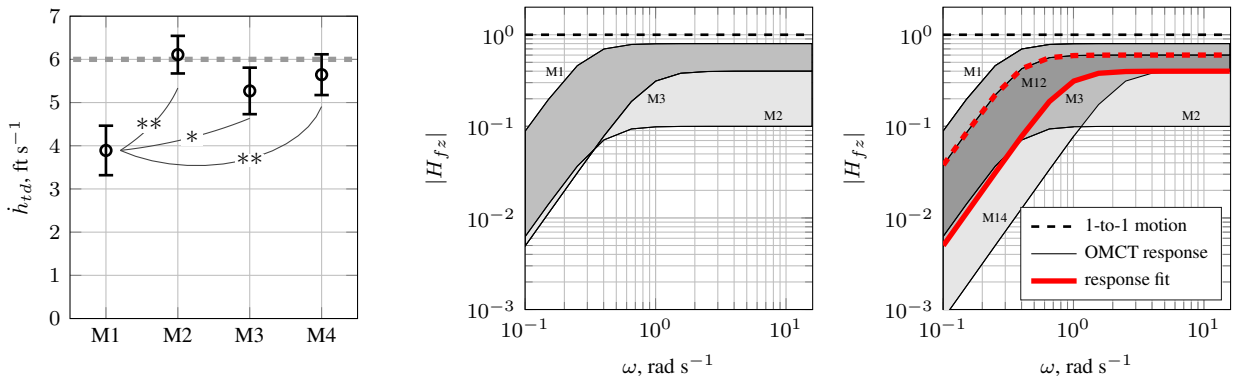

(a) MCUE2014 sinkrate at touchdown. **(b) MCUE2014 fidelity uncertainty boundary.** **(c) Final uncertainty boundary fit.**

Figure 14. Objective motion cueing criteria development.

sponses were defined using the same four steps but using significant differences in false-motion-cue ratings. These cross-coupling responses also defined the low-pass characteristic of the fidelity boundaries for pitch, surge, and sway. Figs. 15 and 16 present the fidelity boundaries based on this approach for the principal responses in the six degrees of freedom and cross-coupling responses, respectively, in red. The areas of satisfactory motion fidelity are light-gray and the areas of unsatisfactory fidelity dark-gray. Both figures also depict the fidelity regions based on a statistical sampling of eight simulators for comparison.[6] Numeric values of the motion fidelity boundaries for each degree of freedom are provided in Tables 3 and 4 in the appendix.

For the pitch OMCT fidelity boundary, significant differences in the number of additional stick shaker activations and maximum pitch rate in the stall recovery (Fig. 10c) were used. Significant differences in roll deviation RMS (Fig. 10a) defined the fidelity boundaries for the roll response. Significant differences in heading deviation RMS and pedal response time in the takeoff task (Fig. 11a) were used for both the sway and yaw OMCT fidelity boundaries. For the heave OMCT fidelity boundary, significant differences in sink rate at touchdown (Fig. 9a) were used to define the fidelity boundary. No experimental differences in task performance were found for defining the surge OMCT fidelity boundary. Instead, the sway fidelity boundary was used.

Significant differences in false-tilt-motion-cue ratings in the sidestep and stall tasks (Figs. 13a and 13b) were used to define the roll-to-sway OMCT fidelity boundary. No motion rating data were available to define the pitch-to-surge fidelity boundary. Instead, this boundary was chosen to be equivalent to the roll-to-sway boundary. For the surge-to-pitch OMCT fidelity boundary, significant differences in false-tilt-motion-cue ratings in the takeoff task were used (Fig. 13c). Due to the lack of appropriate motion-rating data, the sway-to-roll fidelity boundary was chosen to be equivalent to the surge-to-pitch boundary. The surge-to-pitch OMCT fidelity boundary was used to define boundaries for the low-pass filter portion of the pitch and sway principal responses.

VI. Discussion

This paper discusses the final experiment in a set of four to develop objective motion cueing criteria for commercial transport simulators. The first experiment was a quasi-transfer-of-training study evaluating whether different levels of training motion fidelity affect the initial training of commercial transport pilots.[1] This first study provided only a limited number of significant effects of the training motion, with some in the direction not predicted, possibly due to the fact that the general aviation pilots who participated in the study had no prior experience with the aircraft type used.

The second, third and fourth experiments (MCUE2014, MCUE2015, and MCUE2016, respectively) did not focus on training, but on the effects of different levels of motion fidelity on pilots' performance in different flying tasks.[2,3] These experiments used experienced commercial airline transport pilots, representing pilots receiving recurrent training. More significant differences between motion configurations were found in these experiments, and results were more in line with what was expected based on previous research. The last two experiments each refined the criteria uncertainty boundaries developed in the previous experiments.

Each experiment used the same three flying tasks with some minor modifications. The most significant modification for the experiment discussed here was the addition of a tail windshear in the final approach of the sidestep task. Six new motion configurations were used (M11-M16).

VI.A. Effects of Motion on Task Performance and Motion Ratings

In the sidestep landing task, the main objective measure affected by the motion condition was the sink rate at touchdown. Pilots touched down with significantly higher sink rates when the heave motion gain decreased and heave break frequency increased going from M11 to M16. This effect has been observed in previous research.[16] The longitudinal deviation from the desired touchdown point increased marginally significantly going from M11 to M16. This might have been caused by the decreasing heave motion fidelity as well, making it increasingly harder to perform the flare maneuver. Pilots generally touched down long under all motion configurations due to the strong ground effect of the simulated aircraft. Pilots touched down about 4 ft from the centerline on average, less far compared to previous experiments.

Task performance in the approach was not significantly affected by the motion condition. RMS of glideslope and speed deviations did not vary between motion configurations; however, values were much higher in the current experiment compared to the previous experiments. This was caused by the newly introduced tail windshear, which caused the aircraft to lose significant airspeed and altitude. The throttle reaction time after the windshear was also not statistically significantly different between motion configurations. This indicates pilots' ability to compensate for the

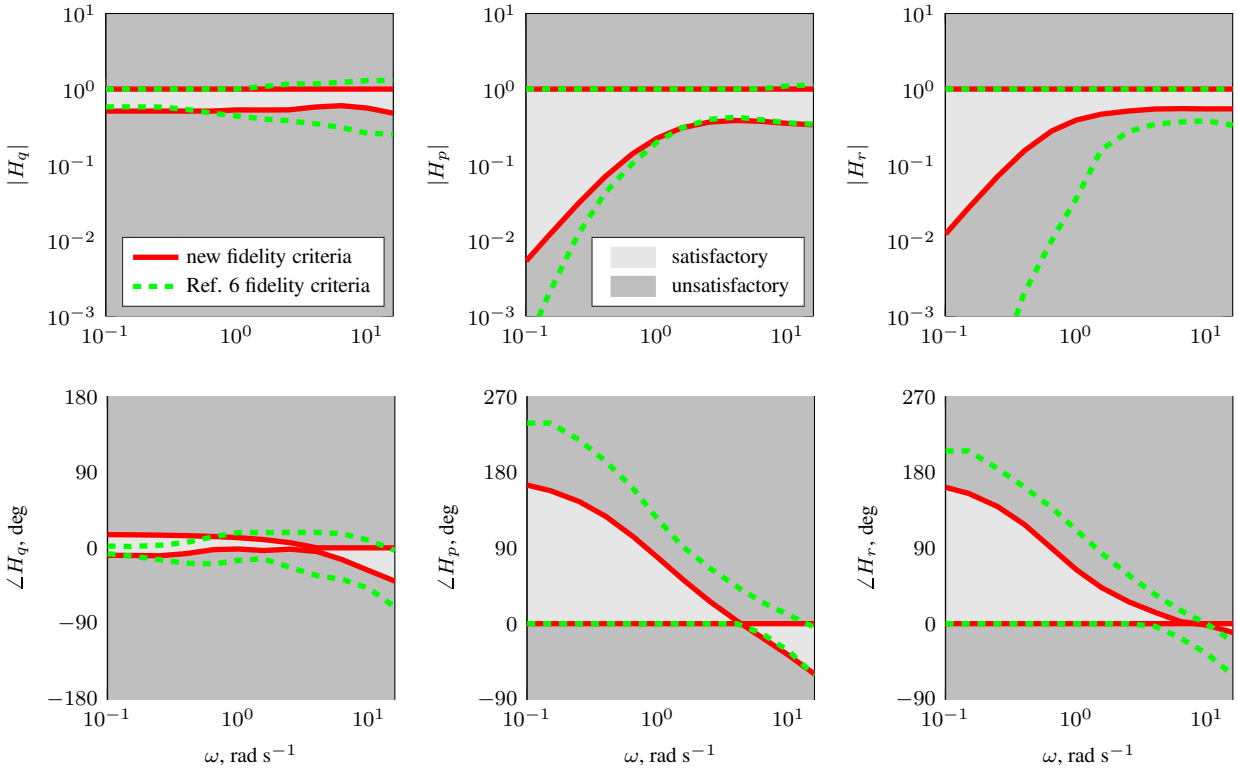

(a) Pitch response to pitch input. **(b) Roll response to roll input.** **(c) Yaw response to yaw input.**

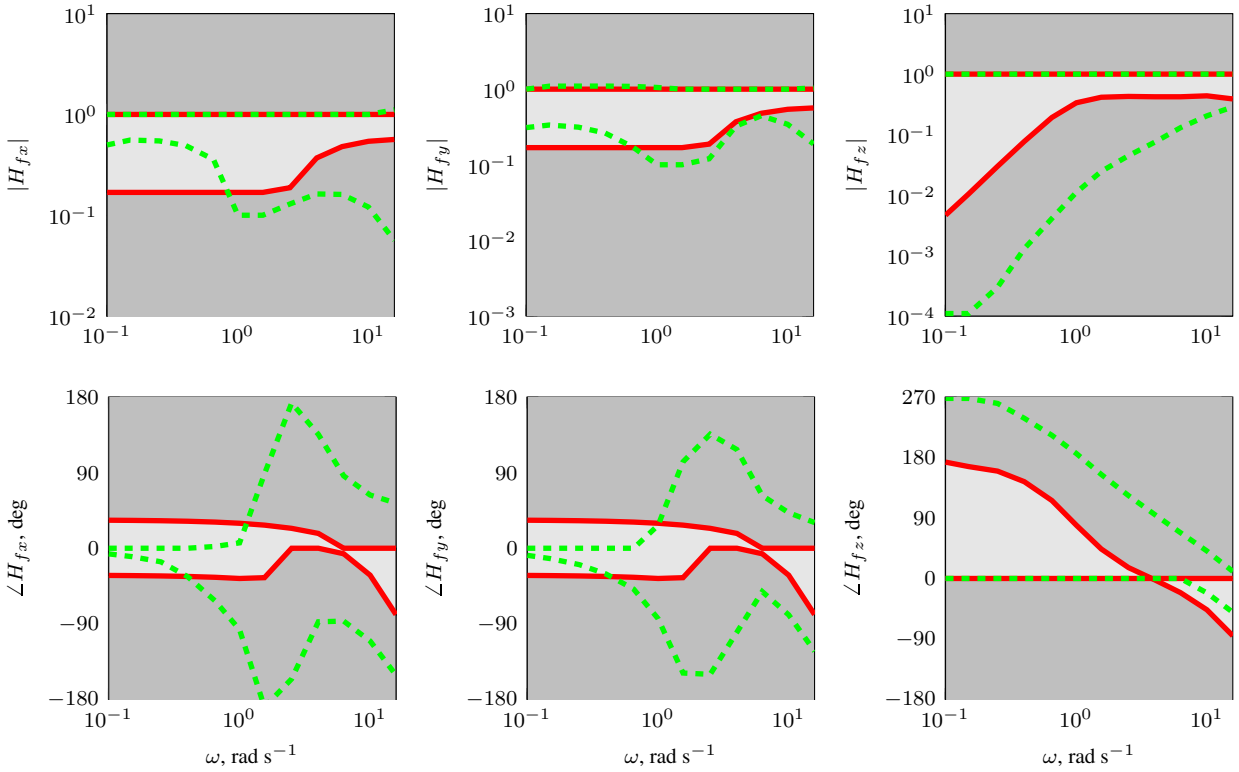

(d) Surge response to surge input. **(e) Sway response to sway input.** **(f) Heave response to heave inpput.**

Figure 15. Objective motion cueing criteria for principal axes.

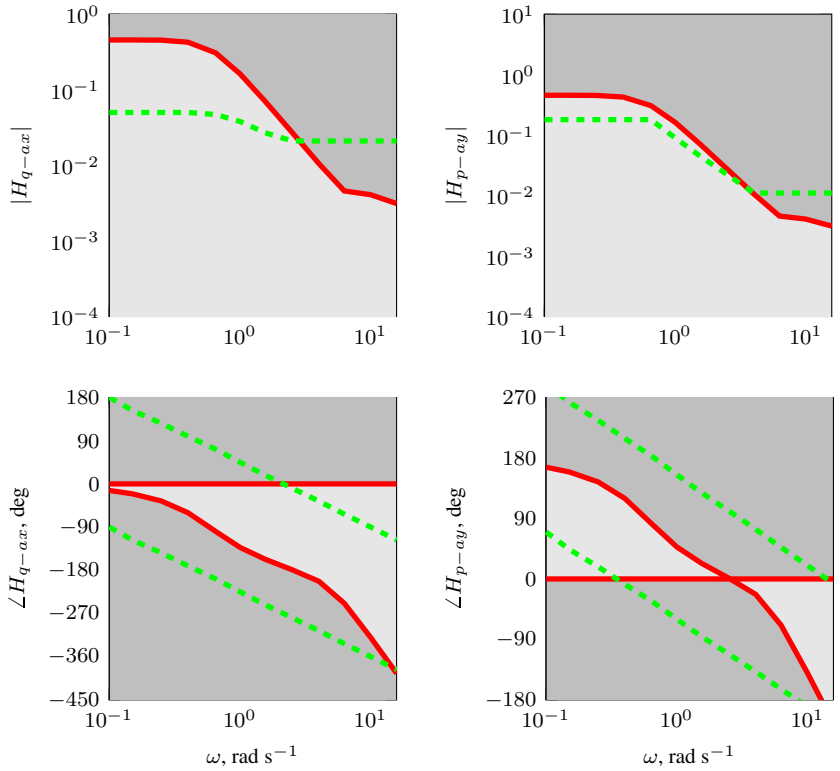

(a) Surge response to pitch input.

(b) Sway response to roll input.

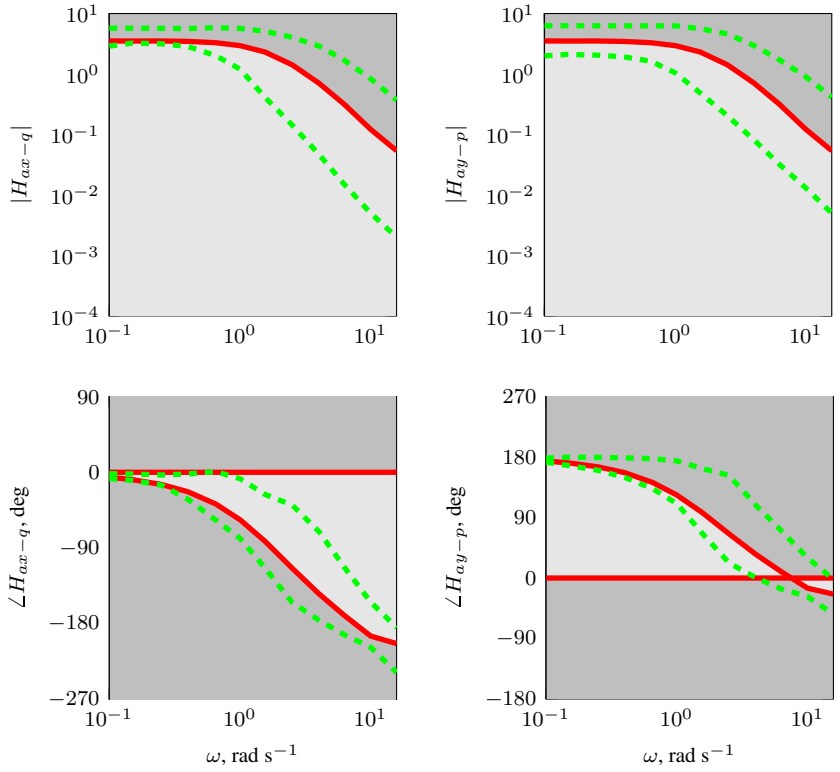

(c) Pitch response to surge input.

(d) Roll response to sway input.

Figure 16. Objective cross-coupling motion cueing criteria.

windshear was not affected by the variations in surge or heave motion fidelity, possibly because pilots mainly focused on airspeed information from the PFD and anticipated the windshear even though its location was randomized.

Roll deviation in the approach to the stall and maximum pitch rate in the stall recovery were significantly affected by the motion condition in the stall task. From M11 to M16, the RMS of the roll angle decreased. Going from M11 to M16, the break frequency of the roll motion filter decreased, resulting in higher fidelity roll motion. In addition, the magnitude of false tilt motion cues increased. This allowed for motion that helped more in keeping the roll angle at the desired value in the approach to the stall. Going from M11 to M16, the RMS of the maximum pitch rate significantly increased. The gain and break frequency of the pitch motion filter increased and decreased, respectively, resulting in higher fidelity pitch motion for M16, the condition with higher maximum pitch rates. However, the fidelity of the heave motion in M11 and M12 was significantly higher compared to M13-M16. In this case, the higher fidelity heave motion helped with regulating pitch oscillations in the stall recovery better. These effects in roll RMS and maximum pitch rate are typically observed in compensatory control tasks when the fidelity of motion feedback is increased.[13] The number of secondary stick shakers in the stall recovery was not significantly affected by motion and was similar to the previous experiment.

In the takeoff task, the RMS of the heading deviation and the reaction time of the initial pedal input after the engine failure were significantly affected by the motion condition. Both increased going from M11-M12 to M13-M15 and then decreased for M16. This suggests that the increase in heading deviation is caused by pilots' delayed response to the engine failure as a result of lower fidelity motion cues. M11 and M12 had the highest fidelity yaw motion (higher yaw gains and lower break frequencies), while M16 had the highest fidelity sway motion (highest sway gain and lowest break frequency). This shows that both yaw and sway motion fidelity had an effect on the pilots' ability to compensate for the engine failure. All takeoff task performance results for the current experiment were comparable to the previous experiment.

Pilots used motion ratings to rate the severity of false tilt motion in each task run. All ratings were between 0%, not noticeable, and 100%, very noticeable and objectionable. In the sidestep and stall tasks, pilots rated the severity of false tilt cues resulting from a lack of turn coordination, while they rated the severity of false tilt cues resulting from residual tilt in the takeoff task. The experiment tested 19 pilots in total; however, motion rating data from only six participants was recorded due to a software error. Statistically significant differences were found across motion conditions for the motion ratings in each task. The perception of false tilt cues correlated well with previous research; that is, if the associated cross-coupling motion response was above the MCUE2015 fidelity criterion based on perception thresholds determined in previous research, pilots rated the false tilt cues as being more severe.

VI.B. Objective Motion Cueing Criteria

Summarizing, we found significant effects of motion on task performance for all three flight tasks. Based on these task performance results, OMCT motion fidelity boundaries were developed similarly to the previous experiments.[2,3] Motion fidelity boundaries were defined by first assigning a task performance result to each degree of freedom. Then, using significant differences in task performance between different motion configurations, fidelity boundaries were defined using the OMCT responses of those motion configurations. If OMCT responses mainly differed in gain, they were used to define fidelity boundaries in the magnitude plot only. The same approach was used for the phase plot fidelity boundaries if the responses mainly differed in phase.

The goal of the current experiment was to refine the initial objective motion cueing criteria developed in the previous experiments. The experiment focused specifically on three issues remaining from the previous experiments: the trade off between motion filter gain versus break-frequency, the trade off between different degrees of freedom, and false tilt motion cues resulting from the cross coupling between degrees of freedom. Fidelity boundaries were developed using task performance and motion rating results directly for all motion-response degrees of freedom, except for the main surge, and pitch-surge and sway-roll cross-coupling degrees of freedom. The surge motion fidelity boundary was chosen to be equivalent to the sway boundary, while the pitch-surge and sway-roll boundaries were chosen to be equivalent to the roll-sway and surge-pitch boundaries, respectively. The resulting motion fidelity boundaries define one side of the satisfactory motion fidelity region. The other side of the region is defined by the magnitude-of-one or zero-phase-error lines. The resulting fidelity boundaries are provided in Figures 15 and 16 by the red lines.

Comparing the new motion fidelity boundaries to the boundaries developed using a statistical sample of eight simulators shows that the new fidelity boundaries are mostly inside those previous boundaries.[6] Especially the lower boundaries of the heave and yaw fidelity regions have a much higher magnitude and lower phase shift. The magnitudes of the rotational to translational cross-coupling boundaries developed using a statistical sample of eight simulators are lower than the magnitudes of the new boundaries below 5 rad/s (Figures 16a and 16b). Note that the cross-coupling boundaries are a result of pilots' perceptual thresholds. This indicates that false tilt motion cues due to a lack of

turn coordination at lower frequencies might not be perceivable in the average hexapod motion simulator. The new translational to rotational cross-coupling boundaries are mostly very similar to the average of the previous boundaries. Note that this means the average hexapod produces rotational rates as a result of residual tilt right at the perception boundary. This result is to be expected as most hexapod motion algorithms use a rate limiter based on the human perceptual threshold in the residual tilt channel. The overall comparison between the developed fidelity boundaries and the data from a statistical sample of eight simulators suggests that some hexapod simulators can possibly produce motion with improved fidelity in several degrees of freedom (except for heave).

The boundaries found here are a result of sometimes relatively small differences in task performance between motion configurations; for example, differences in RMS roll deviation in the stall recovery are 0.5 deg at the most). In addition, no real flight data is available as a baseline condition. A large VMS motion condition was used as a baseline instead. This might raise the question if the fidelity boundaries found here are of any significance for pilot training for real aircraft operations. Future research is required to investigate this issue further. However, the fidelity uncertainty boundaries found here still define motion fidelity regions which allow for improved pilot performance closer to that under motion more similar to real flight, which is a major improvement over the fidelity regions defined using a statistical sample of eight simulators.

The fidelity boundaries were developed using task performance in three challenging tasks designed with the assumption that varying the motion cues would affect pilot performance in these tasks. In addition, a mid-size twin-engine commercial transport aircraft model was used in the VMS. This means that the motion fidelity uncertainty boundaries found here might be specific to these tasks, the aircraft model used, or the VMS. More research is required to validate the fidelity boundaries using other tasks, simulated aircraft, or simulators. For example, Ref. 23 suggests that the fidelity regions might be different for helicopter simulators.

Finally, the OMCT responses of the pitch, surge, and sway degrees of freedom include both low-pass characteristics from residual tilt and high-pass characteristics from principal high-pass filtering, making it difficult to develop intuitive criteria for these degrees of freedom. A possible solution for this might be modifying the OMCT such that the high-pass filter responses in the pitch, surge, and sway degrees of freedom are also considered separately. Optimizing the OMCT was beyond the scope of this research project and should be explored in future research.

VII. Conclusions

This study used the NASA Vertical Motion Simulator with three flight tasks and six different motion configurations to refine objective motion cueing criteria developed in previous experiments. Nineteen experienced airline transport pilots participated, performing each task with all six motion configurations.

Both subjective and objective measures were affected by the motion conditions. For the subjective measures, pilots rated the severity of false tilt cues significantly higher in the conditions when the magnitude of the cross-coupling OMCT response was above the fidelity boundary determined in the previous experiment. Objective task performance results indicate that pilots touched down with significantly higher sink rates and further down the runway in the sidestep task when the heave motion gain decreased and break frequency increased. In the stall task, pilots deviated less from the desired roll angle in the motion conditions with a lower roll motion filter break frequency and higher-magnitude false tilt motion cues. Pilots had a lower maximum pitch rate in the conditions with a higher heave motion gain and lower break frequency. In the takeoff task, pilots deviated less from the desired heading and responded quicker after an engine failure in the motion conditions with higher motion gains and lower break frequencies in the yaw or sway degrees of freedom. Task performance results were in line with previous experiments.

The statistically significant differences found between the motion conditions refined the motion fidelity uncertainty boundaries developed in previous experiments further, resulting in initial fidelity criteria that could be considered for the simulator motion system diagnostic test now required during commercial aircraft simulator approval in the United States. Considering the mean test results of a statistical sample of eight simulators, these initial criteria suggest that some hexapod simulators can possibly produce motion cues with improved fidelity in several degrees of freedom.

Appendix

The VMS motion logic is completely linear in its operating envelope; that is, the only nonlinear element is the motion limiting near the edges of the envelope. The motion configurations of the experiment were tuned such that the chance of hitting motion limits was minimal. Motion filtering on the VMS is performed in the inertial reference frame. Aircraft model accelerations are transformed from the aircraft body reference frame to the inertial reference frame

using small-angle approximations. The logic uses gains and second-order high-pass filters to attenuate accelerations in the translational and rotational degrees of freedom. The motion filter for the lateral degree of freedom y is given by:

$$H_{my} = K_{my} \frac{s^2}{s^2 + 2\zeta_{my}\omega_{my}s + \omega_{my}^2} \tag{1}$$

where s is the Laplace variable, K_{my} is the motion gain, ζ_{my} is the filter damping ratio, and ω_{my} is the filter break frequency. Motion filters for the other degrees of freedom have the same form.

Residual tilt is the process of tilting the simulator cab to provide steady-state longitudinal and lateral accelerations at low frequencies. Residual tilt in the VMS motion logic is normally provided by third-order low-pass filters; however, the filters were changed to second-order low-pass filters for this study, as this is more common in current motion-base flight simulators. Residual tilt in the lateral degree of freedom is provided by:

$$H_{rty} = -K_{my}\frac{K_{rty}}{g} \frac{\omega_{rty}^2}{s^2 + 2\omega_{rty}s + \omega_{rty}^2} \tag{2}$$

Residual tilt in the longitudinal degree of freedom is given by:

$$H_{rtx} = K_{mx}\frac{K_{rtx}}{g} \frac{\omega_{rtx}^2}{s^2 + 2\omega_{rtx}s + \omega_{rtx}^2} \tag{3}$$

In Eq. (2) and Eq. (3) K_{rty} and K_{rtx} are the residual-tilt gains, g is the gravitational acceleration, and ω_{rty} and ω_{rtx} the residual-tilt break frequencies. The motion logic also includes a turn-coordination channel that takes advantage of the large lateral motion capability of the VMS. This channel induces additional lateral motion using roll inputs to reduce false tilt cues. The turn-coordination channel is defined by:

$$H_{tcp} = K_{mp}\, K_{tcp}\, g \frac{1}{s^2 + 2\zeta_{mp}\omega_{mp}s + \omega_{mp}^2} \tag{4}$$

where K_{tcp} is the turn-coordination gain.

More details about the motion configurations of the current experiment are given in Section III. Table 2 provides the motion parameters of all motion configurations and tasks. Refs. 2 and 3 provide more details about the motion configurations of the previous experiments.

Numeric values of the upper and lower uncertainty boundaries for each degree of freedom depicted in Figs. 15 and 16 are provided in Tables 3 and 4. The test numbers refer to the OMCT tests described in ICAO 9625.[4]

Acknowledgments

The authors thank the Vertical Motion Simulator simulation engineers and support personnel who contributed to the four experiments conducted as part of this research project. We especially thank Mike Weinstein, Emily Lewis, Steve Norris, and Nick Riccobono for their valuable contributions in setting up and running the experiments, and for being instructor pilots. We also thank Gordon Hardy for being a test pilot and instructor pilot.

In addition, we would like to thank VMS lab managers Duc Tran and Scott Reardon, and Aerospace Simulation R&D Branch Chief Steve Beard at NASA Ames Research Center for their support and flexibility in using the simulator facilities. We also thank Girish Chachad, SimLabs Outreach Manager, for his administrative support to the project. We would like to thank Dr. Andrew Cheng from the FAA Technical Center for the initial program support and Dr. Huasheng Li for the continued program support.

Finally, we would like to thank the many pilots who participated in the experiments.

References

[1]Zaal, P. M. T., Schroeder, J. A., and Chung, W. W., "Transfer of Training on the Vertical Motion Simulator," *Journal of Aircraft*, Vol. 52, No. 6, Nov.–Dec. 2015, pp. 1971–1984.

[2]Zaal, P. M. T., Schroeder, J. A., and Chung, W. W., "Objective motion cueing criteria investigation based on three flight tasks," *The Aeronautical Journal*, Vol. 121, No. 1236, Feb. 2017, pp. 163–190.

[3]Zaal, P. M. T., Schroeder, J. A., and Chung, W. W., "Refinement of Objective Motion Cueing Criteria Based on Three Flight Tasks," *AIAA Modeling and Simulation Technologies Conference*, American Institute of Aeronautics and Astronautics (AIAA), Jan. 2017.

[4]International Civil Aviation Organization, *ICAO 9625: Manual of Criteria for the Qualification of Flight Simulation Training Devices. Volume 1 – Aeroplanes*, 2009, 3rd edition.

Table 2. MCUE2016 motion configuration parameters.

	Sidestep Task						Stall Task						Takeoff Task					
	M11	M12	M13	M14	M15	M16	M11	M12	M13	M14	M15	M16	M11	M12	M13	M14	M15	M16
motion gains																		
K_{mx}	0.100	0.200	0.300	0.400	0.600	0.800	0.100	0.150	0.200	0.400	0.600	0.800	0.100	0.150	0.200	0.400	0.600	0.800
K_{my}	0.400	0.700	0.400	0.700	0.400	0.700	0.400	0.700	0.400	0.700	0.400	0.700	0.400	0.400	0.400	0.700	0.400	0.700
K_{mz}	0.700	0.600	0.500	0.400	0.300	0.200	0.350	0.500	0.200	0.200	0.200	0.200	0.200	0.300	0.400	0.500	0.600	0.700
K_{mp}	0.400	0.700	0.400	0.700	0.400	0.700	0.400	0.700	0.400	0.700	0.400	0.700	0.400	0.700	0.400	0.700	0.400	0.700
K_{mq}	0.300	0.450	0.600	0.850	0.600	0.850	0.300	0.300	0.600	0.850	0.600	0.850	0.300	0.450	0.600	0.850	0.600	0.850
K_{mr}	0.450	0.850	0.450	0.850	0.450	0.850	0.450	0.850	0.450	0.850	0.450	0.850	0.550	0.650	0.450	0.450	0.450	0.450
filter break frequencies																		
ω_{mx}	0.500	0.650	0.750	0.850	0.950	1.050	0.400	0.500	0.600	1.500	2.500	3.500	0.650	0.750	0.850	1.500	2.500	3.500
ω_{my}	3.000	3.000	1.000	1.000	0.350	0.350	3.000	3.000	1.000	1.000	0.350	0.350	3.000	3.000	1.000	1.000	0.350	0.350
ω_{mz}	0.300	0.400	0.500	2.250	3.000	3.750	1.500	0.900	3.750	3.750	3.750	3.750	3.750	3.000	2.250	0.600	0.500	0.400
ω_{mp}	1.000	1.000	0.450	0.450	0.200	0.200	1.000	1.000	0.450	0.450	0.200	0.200	1.000	1.000	0.450	0.450	0.200	0.200
ω_{mq}	0.850	0.850	0.500	0.500	0.260	0.260	0.850	0.850	0.500	0.500	0.260	0.260	0.850	0.850	0.500	0.500	0.260	0.260
ω_{mr}	0.600	0.600	0.250	0.250	0.080	0.080	0.600	0.600	0.250	0.250	0.080	0.080	0.600	0.080	2.000	2.000	2.000	2.000
filter damping ratios																		
ζ_{mx}	0.707	0.707	0.707	0.707	0.707	0.707	0.707	0.707	0.707	0.707	0.707	0.707	0.707	0.707	0.707	0.707	0.707	0.707
ζ_{my}	1.000	1.000	1.000	1.000	0.707	0.707	1.000	1.000	1.000	1.000	0.707	0.707	1.000	1.000	1.000	1.000	0.707	0.707
ζ_{mz}	0.707	0.707	0.707	0.707	0.707	0.707	0.707	0.707	0.707	0.707	0.707	0.707	0.707	0.707	0.707	0.707	0.707	0.707
ζ_{mp}	0.900	0.900	0.707	0.707	0.707	0.707	0.900	0.900	0.707	0.707	0.707	0.707	0.900	0.900	0.707	0.707	0.707	0.707
ζ_{mq}	0.707	0.707	0.900	0.900	0.900	0.900	0.707	0.707	0.900	0.900	0.900	0.900	0.707	0.707	0.900	0.900	0.900	0.900
ζ_{mr}	0.900	0.900	0.900	0.900	0.900	0.900	0.900	0.900	0.900	0.900	0.900	0.900	0.900	0.900	0.900	0.900	0.900	0.900
residual-tilt parameters																		
K_{tp}	1.000	1.000	1.000	1.000	1.000	1.000	1.000	1.000	1.000	1.000	1.000	1.000	1.000	1.000	1.000	1.000	1.000	1.000
ω_{tp}	3.000	3.000	1.000	1.000	0.350	0.350	3.000	3.000	1.000	1.000	0.350	0.350	3.000	3.000	1.000	1.000	0.350	0.350
K_{tq}	1.200	1.200	1.200	1.200	1.200	1.200	1.200	1.200	1.200	1.200	1.200	1.200	1.200	1.200	1.200	1.200	1.200	1.200
ω_{tq}	0.500	0.650	0.750	0.850	0.950	1.050	0.400	0.500	0.600	1.500	2.500	3.500	0.650	0.750	0.850	1.500	2.500	3.500
turn-coordination gain																		
K_{ty}	0.000	0.000	0.000	0.000	0.000	0.000	0.000	0.000	0.000	0.000	0.000	0.000	0.000	0.000	0.000	0.000	0.000	0.000

Table 3. Criteria uncertainty boundary values for OMCT tests 1 to 5.[4]

			Test 1		Test 2		Test 3		Test 4		Test 5	
			$\|H_q\|$, –		$\|H_{q-ax}\|$, –		$\|H_p\|$, –		$\|H_{p-ay}\|$, –		$\|H_r\|$, –	
		ω, rad/s	Upper	Lower	Upper	Lower	Upper	Lower	Upper	Lower	Upper	Lower
Magnitude	1	0.101	1.000	0.512	0.455	–	1.000	0.005	0.455	–	1.000	0.012
	2	0.151	1.000	0.512	0.455	–	1.000	0.012	0.455	–	1.000	0.027
	3	0.251	1.000	0.512	0.452	–	1.000	0.031	0.452	–	1.000	0.070
	4	0.402	1.000	0.512	0.425	–	1.000	0.069	0.425	–	1.000	0.152
	5	0.653	1.000	0.512	0.307	–	1.000	0.139	0.307	–	1.000	0.280
	6	1.005	1.000	0.531	0.162	–	1.000	0.224	0.162	–	1.000	0.389
	7	1.558	1.000	0.529	0.070	–	1.000	0.307	0.070	–	1.000	0.465
	8	2.513	1.000	0.531	0.027	–	1.000	0.366	0.027	–	1.000	0.512
	9	4.021	1.000	0.579	0.011	–	1.000	0.385	0.011	–	1.000	0.545
	10	6.283	1.000	0.604	0.005	–	1.000	0.375	0.005	–	1.000	0.551
	11	10.003	1.000	0.561	0.004	–	1.000	0.352	0.004	–	1.000	0.547
	12	15.783	1.000	0.480	0.003	–	1.000	0.337	0.003	–	1.000	0.548
			$\angle H_q$, deg		$\angle H_{q-ax}$, deg		$\angle H_p$, deg		$\angle H_{p-ay}$, deg		$\angle H_r$, deg	
		ω, rad/s	Upper	Lower	Upper	Lower	Upper	Lower	Upper	Lower	Upper	Lower
Phase	1	0.101	15.719	-8.867	166.292	0.000	164.980	0.000	166.292	0.000	162.350	0.000
	2	0.151	15.518	-9.068	159.284	0.000	158.396	0.000	159.284	0.000	155.069	0.000
	3	0.251	15.115	-9.471	144.339	0.000	145.380	0.000	144.339	0.000	139.355	0.000
	4	0.402	14.510	-6.813	119.760	0.000	127.562	0.000	119.760	0.000	118.051	0.000
	5	0.653	13.503	-2.087	80.921	0.000	103.292	0.000	80.921	0.000	89.561	0.000
	6	1.005	12.092	-1.415	47.483	0.000	78.428	0.000	47.483	0.000	64.201	0.000
	7	1.558	9.875	-3.188	23.047	0.000	52.579	0.000	23.047	0.000	43.088	0.000
	8	2.513	6.046	-1.594	0.985	0.000	26.225	0.000	0.985	0.000	26.181	0.000
	9	4.021	0.000	-4.479	0.000	-23.012	3.402	0.000	0.000	-23.012	13.424	0.000
	10	6.283	0.000	-14.199	0.000	-68.792	0.000	-16.629	0.000	-68.792	2.574	0.000
	11	10.003	0.000	-27.152	0.000	-140.159	0.000	-37.611	0.000	-140.159	0.000	-1.813
	12	15.783	0.000	-39.653	0.000	-214.748	0.000	-59.987	0.000	-214.748	0.000	-10.461

[5]Code of Federal Regulations, *Flight Simulation Training Device Initial and Continuing Qualification and Use*, Title 14, Part 60.

[6]Hosman, R. J. A. W. and Advani, S. K., "Are Criteria for Motion Cueing and Time Delays Possible? Part 2." *Proceedings of the AIAA Modeling and Simulation Technologies Conference, Boston (MA)*, No. AIAA-2013-4833, 19–22 Aug. 2013.

[7]Sinacori, J. B., "The Determination of Some Requirements for a Helicopter Research Simulation Facility," Tech. Rep. NASA CR-152066, Systems Technology, Inc., Sept. 1977.

[8]Schroeder, J. A., "Helicopter Flight Simulation Motion Platform Requirements," Tech. Rep. NASA/TP-1999-208766, NASA, July 1999.

[9]Stapleford, R. L., Peters, R. A., and Alex, F. R., "Experiments and a Model for Pilot Dynamics with Visual and Motion Inputs," Tech. Rep. NASA CR-1325, NASA, 1969.

[10]Bergeron, H. P., Adams, J. J., and Hurt, Jr., G. J., "The Effects of Motion Cues and Motion Scaling on One- and Two-Axis Compensatory Control Tasks," NASA Technical Note NASA TN D-6110, NASA Langley Research Center, Jan. 1971.

[11]Bray, R. S., "Visual and Motion Cueing in Helicopter Simulation," Technical Memorandum NASA TM-86818, Ames Research Center, Moffett Field (CA), Sept. 1985.

[12]Cooper, D. E. and Howlett, J. J., "Ground Based Helicopter Simulation," *Proceedings of the American Helicopter Society Symposium on Status of Testing and Model Techniques for V/STOL Aircraft, Essington, PA*, 1973.

[13]Jex, H. R. and Magdaleno, R. E., "Roll Tracking Effects of G-vector Tilt and Various Types of Motion Washout," *Fourteenth Annual Conference on Manual Control*, University of Southern California, Los Angeles (CA), 25–27 April 1978, pp. 463–502.

[14]Jex, H. R., Jewell, W. F., and Magdaleno, R. E., "Effects of Various Lateral-Beam-Motion Washouts on Pilot Tracking and Opinion in the "Lamar" Simulator," *Fifteenth Annual Conference on Manual Control*, Wright State University, Dayton (OH), 20–22 March 1979, pp. 244–266.

[15]Bray, R. S., "Initial Operating Experience with an Aircraft Simulator Having Extensive Lateral Motion," Technical Memorandum NASA TM X-62,155, Ames Research Center, Moffett Field (CA), 1972.

[16]Bray, R. S., "Vertical Motion Requirements for Landing Simulation," Technical Memorandum NASA TM X-62,236, Ames Research Center, Moffett Field (CA), Feb. 1973.

[17]van Gool, M. F. C., "Influence of Motion Washout Filters on Pilot Tracking Performance," *Piloted Aircraft Environment Simulation Techniques*, No. AGARD-CP-249, AGARD, 1978, pp. 19–1 – 19–5.

[18]Shirachi, D. K. and Shirley, R. S., "Visual/Motion Cue Mismatch in a Coordinated Roll Maneuver," Contractor Report NASA CR-166259, Computer Sciences Corporation, Nov. 1981.

Table 4. Criteria uncertainty boundary values for OMCT tests 6 to 10.[4]

			Test 6		Test 7		Test 8		Test 9		Test 10	
			$\|H_{ax}\|$, –		$\|H_{ax-q}\|$, –		$\|H_{ay}\|$, –		$\|H_{ay-p}\|$, –		$\|H_{az}\|$, –	
		ω, rad/s	Upper	Lower	Upper	Lower	Upper	Lower	Upper	Lower	Upper	Lower
Magnitude	1	0.101	1.000	0.169	3.521	–	1.000	0.169	3.521	–	1.000	0.005
	2	0.151	1.000	0.169	3.508	–	1.000	0.169	3.508	–	1.000	0.010
	3	0.251	1.000	0.169	3.517	–	1.000	0.169	3.517	–	1.000	0.030
	4	0.402	1.000	0.169	3.460	–	1.000	0.169	3.460	–	1.000	0.077
	5	0.653	1.000	0.169	3.293	–	1.000	0.169	3.293	–	1.000	0.192
	6	1.005	1.000	0.169	2.945	–	1.000	0.169	2.945	–	1.000	0.336
	7	1.558	1.000	0.169	2.310	–	1.000	0.169	2.310	–	1.000	0.415
	8	2.513	1.000	0.188	1.421	–	1.000	0.188	1.421	–	1.000	0.428
	9	4.021	1.000	0.370	0.705	–	1.000	0.370	0.705	–	1.000	0.422
	10	6.283	1.000	0.480	0.316	–	1.000	0.480	0.316	–	1.000	0.422
	11	10.003	1.000	0.542	0.121	–	1.000	0.542	0.121	–	1.000	0.438
	12	15.783	1.000	0.565	0.054	–	1.000	0.565	0.054	–	1.000	0.389
			$\angle H_{ax}$, deg		$\angle H_{ax-q}$, deg		$\angle H_{ay}$, deg		$\angle H_{ay-p}$, deg		$\angle H_{az}$, deg	
		ω, rad/s	Upper	Lower	Upper	Lower	Upper	Lower	Upper	Lower	Upper	Lower
Phase	1	0.101	33.362	-32.375	0.000	-5.858	33.362	-32.375	0.000	-5.858	173.160	0.000
	2	0.151	33.161	-32.576	0.000	-8.767	33.161	-32.576	0.000	-8.767	166.547	0.000
	3	0.251	32.758	-32.979	0.000	-14.550	32.758	-32.979	0.000	-14.550	159.763	0.000
	4	0.402	32.153	-33.584	0.000	-23.279	32.153	-33.584	0.000	-23.279	144.045	0.000
	5	0.653	31.145	-34.592	0.000	-37.721	31.145	-34.592	0.000	-37.721	116.034	0.000
	6	1.005	29.735	-36.002	0.000	-56.625	29.735	-36.002	0.000	-56.625	79.246	0.000
	7	1.558	27.518	-35.059	0.000	-82.213	27.518	-35.059	0.000	-82.213	43.866	0.000
	8	2.513	23.689	0.000	0.000	-114.285	23.689	0.000	0.000	-114.285	16.243	0.000
	9	4.021	17.643	0.000	0.000	-144.679	17.643	0.000	0.000	-144.679	0.000	-2.335
	10	6.283	0.000	-6.581	0.000	-170.418	0.000	-6.581	0.000	-170.418	0.000	-21.098
	11	10.003	0.000	-32.042	0.000	-195.016	0.000	-32.042	0.000	-195.016	0.000	-46.600
	12	15.783	0.000	-78.989	0.000	-203.989	0.000	-78.989	0.000	-203.989	0.000	-85.320

[19]Anonymous, *Military Specification - Flying Qualities of Piloted Airplanes*, Department of Defense, U.S.A., Washington, D.C., MIL-F-8785C, Nov. 1980.

[20]Beard, S. D., Reardon, S. E., Tobias, E. L., and Aponso, B. L., "Simulation System Optimization for Rotorcraft Research on the Vertical Motion Simulator," *Proceedings of the AIAA Modeling and Simulation Technologies Conference, Minneapolis (MN)*, No. AIAA-2012-4634, 13–16 Aug. 2012.

[21]Field, A., *Discovering Statistics Using SPSS*, ISM Introducing Statistical Methods, SAGE Publications Ltd., 1 Oliver's Yard, 55 City Road, London EC1Y 1SP, 2nd ed., 2005.

[22]Groen, E. L. and Bles, W., "How to use body tilt for the simulation of linear self motion," *Journal of Vestibular Research*, Vol. 14, No. 5, Jan. 2004, pp. 375–385.

[23]Jones, M., White, M., Fell, T., and Barnett, M., "Analysis of Motion Parameter Variations for Rotorcraft Flight Simulators," *Proceedings of the AHS 73rd Annual Forum*, AmericanHelicopter Society International, Inc., May 2017.